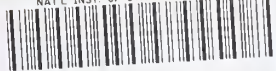


Reference

NBS
Publi-
cations

NAT'L INST. OF STAND & TECH R.I.C.



A11104 346783

NBSIR 78-1541

Techniques for the Measurement of Acoustic Impedance of Asphalt

P. A. Mansbach and C. I. Holmer

Acoustical Engineering Division
Center for Mechanical Engineering and
Process Technology
National Engineering Laboratory
National Bureau of Standards
Washington, D.C. 20234

October 1978

Prepared for
**U.S. Environmental Protection Agency
Office of Noise Abatement and Control**

QC
100
.U5E
78-1541
1978

National Bureau of Standards
MAY 14 1978
NOT ACC. FILE
GRIDE
USG
11/20/77

NBSIR 78-1541

TECHNIQUES FOR THE MEASUREMENT OF ACOUSTIC IMPEDANCE OF ASPHALT

P. A. Mansbach and C. I. Holmer

Acoustical Engineering Division
Center for Mechanical Engineering and
Process Technology
National Engineering Laboratory
National Bureau of Standards
Washington, D.C. 20234

October 1978

Prepared for
U.S. Environmental Protection Agency
Office of Noise Abatement and Control

The Environmental Protection Agency has contributed to the development of the data included in this report but the conclusions and recommendations are solely the responsibility of the National Bureau of Standards.



U.S. DEPARTMENT OF COMMERCE, NBSIR 78-1541

U.S. DEPARTMENT OF COMMERCE, Juanita M. Kreps, Secretary
Dr. Sidney Harman, Under Secretary
Jordan J. Baruch, Assistant Secretary for Science and Technology
NATIONAL BUREAU OF STANDARDS, Ernest Ambler, Director

ABSTRACT

Five techniques were used for the measurement of the very high specific acoustic impedance of an asphalt surface. These techniques are: Impedance Tube, Pure-Tone Traverse, Pulse-Echo, Broad-Band Cross-Correlation, and Direct Accelerometer Measurement. These techniques, as used in the present investigation, are described and evaluated in some detail, and the results of the measurements are presented. Of the five techniques, the broad-band cross-correlation proved to be the most effective, and is readily capable of even further improvement. The value of the specific acoustic admittance ratio, $\rho c/z$, (averaged over frequencies) of the sealed asphalt surface obtained with this technique is .007. The effects of atmospheric wind and temperature gradients on ray propagation, and spherical wavefront corrections to plane-wave reflection, are derived theoretically. These refinements are necessary to realize the full potential of the broad-band measurement technique. Effects of the finite test surface impedance on source emission measurements are discussed. Variations in measured sound levels of the order of 1-2 dB due to differing impedances at different test site surfaces are considered likely, given the limited data on asphalt impedance presently available.

ACKNOWLEDGMENTS

The authors wish to acknowledge the contributions of Donald S. Blomquist and Charles O. Shoemaker for their assistance in the Sandusky field measurements, Dennis D. Toth for conducting the direct accelerometer measurements, Carl R. Voorhees for assistance in data reduction, and other members of the Acoustical Engineering Division for assistance both in the laboratory and through discussions.

We wish to thank Dr. Peter Baade* for discussion and for the suggestion of making the direct accelerometer measurement.

The impedance tube measurements were conducted under the direction of Y. M. Chang,** in cooperation with International Harvester, Inc.

* Research Division, Carrier Corp., Syracuse, NY

** U.S. EPA Enforcement Div., Sandusky, OH

CONTENTS

1.	INTRODUCTION1
1.1.	Rationale1
1.2.	Definitions and Assumptions2
1.3.	Scope of Experiment and Analysis4
1.3.1.	Experiment4
1.3.2.	Further Analysis5
2.	IMPEDANCE TUBE MEASUREMENTS6
2.1.	Description of Technique6
2.2.	Advantages and Limitations6
2.3.	Experiment7
2.4.	Results7
3.	PURE-TONE TRAVERSE9
3.1.	Glancing Angle Geometry9
3.2.	Description of Traverse Technique	10
3.3.	Advantages and Limitations	11
3.4.	Experiment	12
3.5.	Results	12
4.	PULSE-ECHO MEASUREMENTS	16
4.1.	Description of Experiment	16
4.2.	Advantages and Limitations	16
4.3.	Experiment	17
4.4.	Results	19
5.	BROAD-BAND CROSS-CORRELATION	22
5.1.	Description of Technique	22
5.1.1.	Data Collection	22
5.1.2.	Correlogram Features	22
5.1.3.	Extraction of Reflection Coefficient	24
5.2.	Advantages and Limitations	24
5.3.	Experiment	26
5.3.1.	Configuration	26
5.3.2.	Locations of Source and Microphones	30
5.4.	Initial Data Reduction	30
5.5.	Final Data Reduction and Results	32
5.6.	Analysis of Delay Times	32
5.7.	Sources of Error	34
5.8.	Corrections for Wind Gradient	37
5.9.	Corrections for Temperature Gradient	38

6.	DIRECT ACCELEROMETER MEASUREMENT	39
6.1.	Description of Technique	39
6.2.	Advantages and Limitations	39
6.3.	Experiment	40
6.4.	Results	40
6.5.	Validation	44
7.	EFFECTS OF WIND AND TEMPERATURE GRADIENTS	45
7.1.	Description of Effects	45
7.2.	"Non-Effect" of Uniform Wind	45
7.3.	Fermat's Principle	48
7.4.	Time-of-Flight Lemma	48
7.5.	Effect on Propagation Time Difference	50
7.6.	Effect on Angle of Incidence	51
7.7.	Focusing Effect	55
7.8.	Wind Profile	59
8.	SPHERICAL WAVEFRONT CORRECTIONS	61
8.1.	Correction Expressions	61
8.2.	Application to Impedance Measurement	62
9.	EFFECT OF SURFACE IMPEDANCE ON SOURCE EMISSION MEASUREMENTS	65
9.1.	Assumptions	65
9.2.	Real Admittance	65
9.3.	Complex Admittance	67
10.	CONCLUSIONS	69
10.1.	Evaluation of Techniques	69
10.2.	Results of Impedance Measurement	71
10.3.	Effect of Impedance on Source Emission Measurements	73
10.4.	Further Possibilities	73
Appendix A.	Symbols	75
B.	Use of Admittance in Favor of Impedance	80
C.	Derivation of Cross-Correlation Functions	81
D.	Exact Ray Path Integral	85
REFERENCES.	86

LIST OF FIGURES

		Page
Figure 1.	Ray Diagram for Glancing Angle Geometry	3
Figure 2.	Sketch of Pure-Tone Traverse	13
Figure 3.	Block Diagram for Pure-Tone Traverse	14
Figure 4.	Block Diagram for Pulse-Echo	18
Figure 5.	Example of Cross-Correlogram	23
Figure 6.	Source and Microphone Layout - Plan View	27
Figure 7.	Source and Microphone Layout - Elevation	28
Figure 8.	Block Diagram for Broad-Band Cross-Correlation - Data Collection	29
Figure 9.	Block Diagram for Broad-Band Cross-Correlation - Data Reduction	31
Figure 10.	Examples of Predicted Correlograms	36
Figure 11.	Sketch of Direct Accelerometer Measurement	41
Figure 12.	Block Diagram for Direct Accelerometer Measurement	42
Figure 13.	Output from Direct Accelerometer Measurement	43
Figure 14.	Ray Geometry in Comoving Coordinates	46
Figure 15.	Ray Paths in the Presence of a Wind Gradient	52
Figure 16.	Ray Diagram for Focusing Effect	56
Figure 17.	Graph of Function $F(a)$, for Real a (Eq. 8-2c)	63



1. INTRODUCTION

1.1. Rationale

Noise emission measurements for several kinds of equipment are frequently conducted at large outdoor test sites. A primary example is the measurement of noise from new medium and heavy trucks, as specified in the U.S. Environmental Protection Agency Regulation limiting their noise emissions.[1]*

In applying such a regulation, it is necessary to be assured of a high degree of precision in the measurement procedure. Two areas of variability have been pointed out [2] which may affect the precision of test procedures of this type. These areas are variability between measurement sites--including the geometry of the test surface, unevenness in the surface, and differences in the acoustic properties of the surface -- and variations in weather conditions.

This study addresses the question of the acoustic properties of the test site surface, with primary emphasis on the measurement of these acoustic properties. The surfaces of concern are "hard" test sites, specifically asphalt or concrete. There has been very little attention in the literature to the measurement of surface reflection properties when the normal reflection coefficient (defined below) may be as high as 0.99. Yet even for surfaces this hard, the reflection coefficient at glancing angles is expected to be much less -- e.g., .90 at 5° incidence -- so that the small remaining absorption may routinely introduce differences of the order of 1-2 dB in source emission measurements performed at different test sites.

It may thus be desirable to set quantitative bounds on the acoustic characteristics of the surface. Surface impedance measurements performed at a variety of test sites and under differing pad temperature conditions would provide some estimate of the variability of the surface impedance, and thereby provide an estimate on the variability of source emission measurements due to site variation. The data base thus acquired would help to specify a pad surface impedance qualification requirement.

A clear prerequisite for both a site characterization survey and a possible qualification requirement is the development of a practical and sufficiently accurate procedure for measuring these surface reflection characteristics.

*Numbers in square brackets identify references which are listed at the end of this report.

1.2. Definitions and Assumptions

By analogy with optics and with underwater acoustics, it may be expected that surface reflection will be specular (as opposed to diffuse), since the surface roughness is small compared to the wavelengths of audible sound.

Thus, the acoustic properties of the surface may be described by a complex reflection coefficient C_r , whose magnitude and phase represent the amplitude and phase of the reflected wave relative to the incident wave. In general, C_r depends both on frequency and angle of incidence. Some authors restrict C_r to plane waves. In this paper, C_r is defined for an omnidirectional point source above a plane by writing the sound pressure as

$$p = \text{const} \times \left\{ \frac{e^{ikR_1}}{4\pi R_1} + C_r \frac{e^{ikR_2}}{4\pi R_2} \right\} e^{-i\omega t}, \quad (1-1)$$

where R_1 and R_2 are the distances of the microphone from the source via the direct and reflected ray paths, respectively (see Figure 1). C_r is a complex number; its magnitude and phase will be denoted by $|C_r|$ and ϕ_r , respectively. Note the phase convention.

A somewhat more abstract characterization of the surface is given by its specific acoustic impedance z , a boundary condition defined as the (complex) ratio of the acoustic pressure to the normal particle velocity at the surface, expressed as a function of frequency. (For a discussion of impedance models see (e.g.) Ref. [3].) An acoustically "hard" surface corresponds to a large value of $|z|$ relative to ρc , the specific acoustic impedance of air.

A further simplification is introduced by assuming a locally reacting surface, that is, assuming that waves propagating within the surface itself do not significantly affect the reflection of waves from the surface. With this assumption, the plane wave reflection coefficient is

$$C_{rp} = \frac{\sin \alpha - \beta}{\sin \alpha + \beta}, \quad (1-2)$$

where the subscript p denotes that C_{rp} is strictly applicable only for plane waves. Here α is the angle of incidence of the plane wave, measured from the horizontal, and

$$\beta = \rho c / z \quad (1-3)$$

is the specific acoustic admittance ratio of the surface (ρc is the specific impedance of air). (The use of β rather than z is discussed in Appendix B). For a "hard" surface, $|\beta| \ll 1$. Note that, for a locally reacting surface, β is

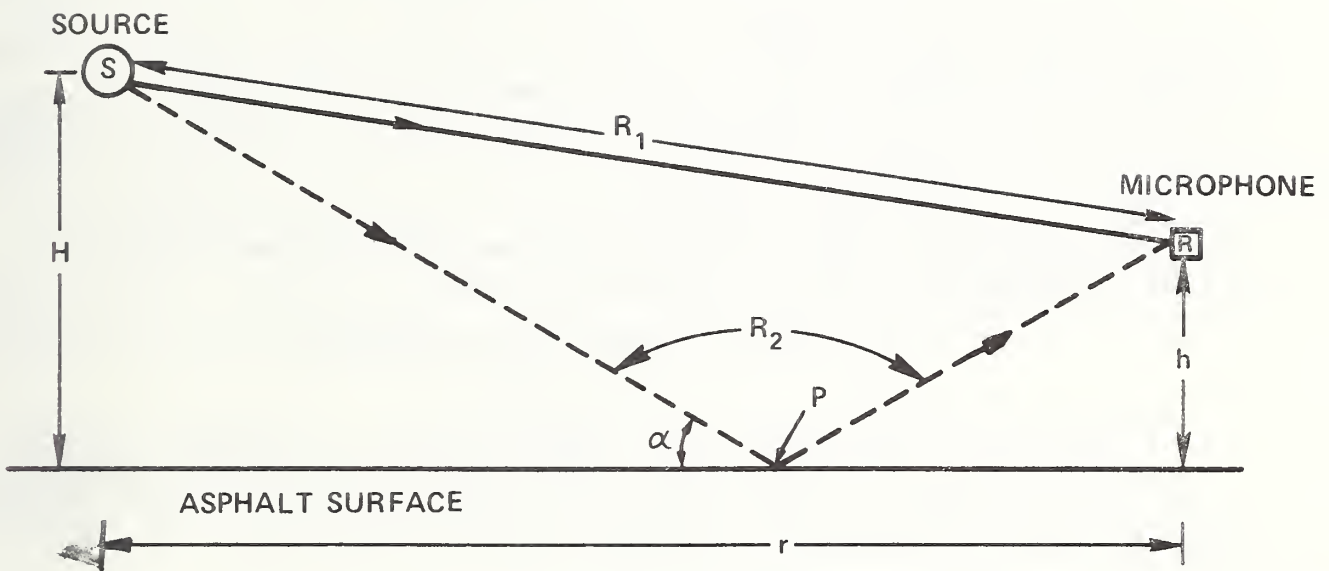


Figure 1. Ray Diagram for Glancing Angle Geometry
 (Note that R_2 is the combined length of both legs.)

by definition independent of the angle of incidence. The validity of this assumption (of local reaction) may be questioned; certainly for porous materials serious doubts have been raised [4,5].

Corrections must be applied to the above expression for C_r (Eq. 1-2) to obtain C_r , defined by Eq. (1-1), since the waves described by Eq. (1-1) are not in fact plane. These corrections will be evaluated in Section 8. For the measurements of impedance performed in this study, these corrections are generally less than 10%, and will be ignored for the time being. Thus, although C_r is used (properly) in the expressions describing measured reflected amplitudes, β will be deduced by assuming $C_r \approx C_{rp}$. For situations in which β becomes comparable to $\sin \alpha$, however, the spherical wavefront corrections must not be neglected.

Throughout this report, it will be assumed that C_r and β are independent of signal amplitude; i.e., that the surface responds linearly to incident radiation.

In this study ray diagrams such as that in Figure 1 have been used to derive the data reduction equations. There is thus the tacit assumption that the reflection occurs at a single point on the surface, and that the properties of this point are being measured. In fact, as with any wave phenomenon, reflections are not point phenomena but involve a finite extent of the surface. The exact area of surface participating in the reflection process has not been determinable in this study. As long as the surface itself is uniform over the interaction area, the properties measured can be used to describe the surface. Section 8 examines the effect of the actual wave nature of the reflection process, provided the surface is uniform and flat.

1.3. Scope of Experiment and Analysis

1.3.1. Experiment

Five techniques were used in this study to measure the specific acoustic impedance of a surface. These techniques have been evaluated in terms of their utility, under field conditions, in measuring very high values of impedance.

The techniques examined are:

- 1) Impedance Tube
- 2) Pure-Tone Traverse
- 3) Pulse-Echo
- 4) Broad-Band Cross-Correlation
- 5) Direct Accelerometer Measurement

The principal measurement site was the asphalt test pad surface at the U.S. Environmental Protection Agency Noise Enforcement Facility in Sandusky, Ohio. Tests were performed at this site both before and after the asphalt had been sealed. The direct accelerometer measurements were added to this study some time later, and these were performed in a parking lot at the National Bureau of Standards, for evaluation of the technique.

In the following five sections, each of these techniques will be described, its limitations discussed, and the measurement results presented. It should be emphasized that it is the techniques as used in this study which are being compared. In several instances modifications to these techniques will be suggested, which offer the potential of improved accuracy or precision, or easier application of these techniques to measuring the acoustic properties of asphalt outdoors.

1.3.2. Further Analysis

It will be seen that the broad-band technique provided the most precise measurement of the magnitude of the specific impedance, and offers promise of further refinement. Realization of the full potential of this measurement technique requires consideration of effects generally assumed "small," namely the effects of wind and temperature gradients on acoustic ray propagation, and the effect of the spherical (nonplanar) nature of the wavefront on the sound field at the measurement position.

As a result, these two effects have been examined in some detail in Sections 7 and 8. Although fairly technical and theoretical in their approach, these two sections provide the needed foundation for the analyses discussed in earlier sections.

In Section 9 the effects of the finite specific impedance on routine source emission measurements are briefly investigated. Errors of 1-2 dB are not unlikely, assuming a specific admittance ratio less than .01. Further impedance measurements might indicate a lower value of the admittance ratio, which would reduce this measurement uncertainty proportionately.

The final section summarizes the results of this study, including the principal advantages and disadvantages of the five impedance measurement techniques.

2. IMPEDANCE TUBE MEASUREMENTS

2.1. Description of Technique

The impedance tube measurement is the conventional technique for measuring surface impedance under normal incidence conditions [6,7]. The apparatus consists of a long cylinder with a sound source at one end. The opposite end terminates in the sample surface to be measured. The source is excited with a pure tone, resulting in a standing wave pattern in the tube. The locations of the minima relative to the sample surface are related to the phase change at reflection, and the difference in level between maximum and minimum (the standing-wave ratio) is determined by the attenuation at reflection. Thus

$$|C_r| = \frac{10^{\Delta L/20} - 1}{10^{\Delta L/20} + 1} \quad (2-1)$$

$$\phi_r = \pi - 4\pi f D_1 / c \quad (2-2)$$

where ΔL is the standing wave ratio in decibels, D_1 is the distance from the surface to the first minimum, f is the frequency of the tone, and c is the speed of sound. The reflection coefficient C_r has been written as

$$C_r = |C_r| e^{i\phi_r} \quad (2-3)$$

From C_r , the specific acoustic admittance ratio β is computed using

$$\beta = \frac{1 - C_r}{1 + C_r} \quad (2-4)$$

obtained from Eq. (1-2) for the case of normal incidence.

2.2 Advantages and Limitations

Clearly this technique measures the normal incidence reflection coefficient, and it is still necessary to validate experimentally a relation between the normal incidence data and the reflection coefficient at the glancing angles of interest, such as is provided by the locally reacting point impedance model.

The use of the impedance tube to measure acoustically hard surfaces is limited by the size of the standing-wave ratios which can be measured accurately. To measure a value of the specific admittance ratio $|\beta|$ of .01, for example, it is necessary to measure a standing-wave ratio of 40 dB. Yet $|\beta| = .01$ (and real) gives rise to 2 dB of attenuation when reflection occurs at a glancing angle of 5° , and thus may significantly affect the results of source emission measurements.

Further, for high values of specific impedance, the phase of the deduced specific impedance is extremely sensitive to slight errors in the measurement of D_1 , the position of the minimum. Thus measurement of the phase of the specific impedance is not reliable. Yet knowledge of this phase may be required to deduce glancing angle reflection coefficients from the normal incidence data.

The limitations on measuring high standing wave ratios may be caused by losses in the walls of the impedance tube, disturbance of the field in the tube due to insertion of the microphone probe, misalignment of the tube resulting in excitation of cross modes, and noise, both acoustical and electronic. Some of these difficulties can be minimized; for example, narrow band filtering can effectively eliminate noise as a problem. Other limitations may be ameliorated to varying degrees by yet greater care in the experiment, or by using more sophisticated instrumentation. Using conventional techniques, however, it was found to be difficult to measure standing wave ratios greater than about 40 dB consistently and reliably, under field conditions.

The impedance tube is attractive in that the measurements are conducted in an enclosed space and are unaffected by the wind.

2.3. Experiment

Impedance tube measurements were performed under the direction of Y. M. Chang in cooperation with International Harvester, Inc., at the Sandusky test site on August 24-25, 1976, before the asphalt had been sealed, and again on September 8-9, 1976, after sealing. These measurements are reported on in detail in a separate document. [8]

2.4. Results

Averaged results are presented in Table 1. It is not clear whether the data scatter represented by the standard deviations reflects measurement imprecision or actual spatial variation of the surface specific impedance.

The experience obtained in the field confirmed the expectation that standing wave ratios above about 40 dB could not be reliably and consistently measured with the apparatus used. As a result, values of $|\beta|$ much below .01 could not be reliably measured. Further, the measurement of the phase of β was severely limited by uncertainties in the position of the acoustic center of the microphone probe, uncertainty in the position of the surface itself, and imprecision in the measurement of the distance between them. The scatter in the measurements of $\arg \beta$ is comparable to that which would be obtained from the selection of random numbers in the range -90° to $+90^\circ$.

Table 1
Summary of Impedance Tube Data*

Frequency (Hz):	125	250	500	1000	1600
Unsealed					
$ \beta $ (averaged)	.029	.023	.022	.029	.036
std dev	.010	.006	.006	.011	.010
arg β (averaged)	+14°	+ 8°	+13°	+27°	+30°
std dev	16°	16°	25°	31°	35°
Sealed					
$ \beta $ (averaged)	.009	.008	.012	.020	.023
std dev	.002	.005	.007	.008	.013
arg β (averaged)	+21°	+ 8°	+72°	+79°	+60°
std dev	45°	58°	22°	6°	43°

* Data collected and reduced under the direction of Y. M. Chang (U.S.E.P.A.), in cooperation with International Harvester, Inc. See ref. [3].

Notes: Values are averages of measured $|\beta|$ and arg β taken at 15 positions. Standard deviations are computed from the scatter of the 15 individual data points.

3. PURE-TONE TRAVERSE

3.1. Glancing Angle Geometry

Three of the techniques used in this study--pure-tone traverse, pulse-echo, and broad-band cross-correlation--measure reflection coefficients at glancing angles directly. In this report the term "glancing angle" refers to angles of incidence α less than about 20° , measured from the horizontal. This is the range of angles of incidence typically encountered in passby test configurations.

Figure 1 shows a ray diagram applicable to all three glancing-incidence techniques. A sound source at S emits a signal, and a microphone at R receives both a direct signal and a signal reflected off the surface under test.

The following quantities are defined for the geometry of Figure 1:

H source height

h microphone height

r horizontal distance from source to microphone

$R_1 = [r^2 + (H-h)^2]^{1/2}$ distance travelled by direct ray (SR on Fig. 1)

$R_2 = [r^2 + (H+h)^2]^{1/2}$ distance travelled by reflected ray (SPR on Fig. 1)

$\delta_R = R_2 - R_1$ path length difference

α angle of incidence, measured from the surface.

Note that $\tan \alpha = (H+h)/r$. The path length difference δ_R may be readily computed:

$$\delta_R = R_2 - R_1 = 2Hh/r', \quad (3-1a)$$

where

$$r' = (R_2 + R_1)/2 \approx r \left(1 + \frac{H^2 + h^2}{2r^2} \right). \quad (3-1b)$$

Terms smaller by another factor of $4 Hh/r^2$ have been ignored in Eq. (3-1b). (For the glancing angle geometry [$\alpha \leq 20^\circ$] $4 Hh/r^2 < 0.1$ and these terms represent corrections to δ_R of less than 1%.)

All three glancing angle techniques measure the reflection coefficient C_r defined by Eq. (1-1). In all cases, the specific admittance ratio β is obtained from C_r , using the locally reacting point impedance model Eq. (1-2), and assuming $C_r \approx C_{rp}$ (the plane wave reflection coefficient); thus

$$\beta = \frac{1-C_r}{1+C_r} \sin \alpha \quad (3-2)$$

Thus values of β , obtained from reflection coefficients measured at different angles of incidence, may be compared directly.

In fact, however, C_r is the quantity of physical interest, i.e., the quantity which directly expresses the result of a source emission measurement (see Eq. (1-1)). Thus, measurements of C_r made at the glancing angles of interest do not depend on the validity of the point impedance model for their utility in assessing source emission measurements made at the same angles.

3.2. Description of Traverse Technique

The pure-tone traverse technique is similar in concept to the impedance tube, except that the reflection coefficient at glancing angles is measured directly. [9,10]

The source is a continuous pure tone, and the microphone is moved along the reflected ray path (PR in Fig. 1). As for the impedance tube measurement, the positions of the minima along the traversed path are used to compute the phase shift at reflection, and the difference between maximum and minimum levels is a measure of the attenuation at reflection. By following the reflected ray, the angle of incidence is kept fixed.

For the traverse, the phase shift ϕ_r is given by

(3-3)

$$\phi_r = \pi - 2\pi \delta_R / \lambda$$

where

δ_R is the path length difference defined in Eq. (3-1),

$\lambda = c/f$ is the wavelength of the pure tone,

f is the pure tone frequency, and

c is the speed of sound in the air.

Having first determined the phase shift ϕ_r from Eq. (3-2), the magnitude of the reflection coefficient is determined from

$$10^{\Delta L/10} = \frac{\left\{ \left(1 + \frac{h}{H}\right)^2 - \frac{\delta_R}{r} \right\} \left\{ 1 + 2|C_r| \cos \phi_r + |C_r|^2 \right\}}{\left\{ \left(1 - |C_r|\right)^2 + \frac{\delta_R}{r \left(1 + \frac{h}{H}\right)^2} (1 - |C_r|)^2 \right\}} \quad (3-4)$$

where ΔL is the difference between maximum and minimum sound pressure levels. The specific admittance ratio β is obtained from C_r using Eq. (3-2).

3.3. Advantages and Limitations

Since C_r is measured at glancing angles, the same value of β results in lower values of $|C_r|$ and smaller values of ΔL than for the impedance tube measurement. The absence of any enclosure, however, means that values of ΔL as large as could be measured in an impedance tube cannot in practice be measured using the traverse.

Thus the major limitation of the traverse technique is again due to the highest ΔL that can be measured. Under normal field conditions, with even a small amount of wind, the associated wind turbulence refracts the sound field irregularly, causing the precise location of the minimum to move around and producing rapid fluctuations in level at the microphone [11]. It is the authors' experience that a wind speed as low as 8 km/hr (5 mph) would limit the measurable ΔL to 20-25 dB regardless of how long one averages. This corresponds to values of $\beta > .015$.

The traverse technique is quite accurate, however, in measuring the phase shift ϕ_r . The estimated precision of $\pm 5^\circ$ results from uncertainties in the microphone position of ± 3 mm. Additional uncertainties result from the presence of wind and temperature gradients.

To the extent these gradients are known, they can be corrected for, as discussed in Section 7. Corrections are also required for the spherical wave-front; these are derived in Section 8.

The sensitivity of the deduced phase of β to the measured location of the minimum is not nearly as serious as for the impedance tube measurement, since at glancing angles the reflection coefficient $|C_r|$ is not so close to 1.

The traverse is limited to the higher frequencies since a pressure minimum occurs only when the path length difference is large enough: $\delta_r \geq \lambda/2$, for $\phi_r = 0$. With the configuration used in this study, frequencies were limited to 1 kHz and above.

A major deterrent in using the traverse technique was that the traversing apparatus used was cumbersome and difficult to set up with the required precision. Once set up, the traverse can be used to collect data at only one angle of incidence and only one reflection point on the surface. Each change in these parameters requires knock down and reassembly of the apparatus. Also, noise from the traverse motor interfered with determining the location of the minimum, let alone the measurement of the sound pressure level there. Performing the traverse by hand, perhaps using a string to define the traverse path, seems to be a lot easier, particularly if the precise angle of incidence can be determined a posteriori from the measured values of h and r , without requiring that it take on a predetermined value.

3.4. Experiment

The pure-tone traverse measurement was conducted at Sandusky on August 27, 1976, on unsealed asphalt. The mechanical setup is shown in Fig. 2, and a block diagram of the electronics is presented in Fig. 3.

The source transducer consisted of 2 Phillips 5060W8 speakers, one on each end of a 75 mm long by 200 mm diameter plastic cylinder. Lab tests had shown this source to be fairly non-directional (within ± 0.5 dB) within the angles of interest, for frequencies below 2.5 kHz. The source was mounted at a height of 1.2 m (4 ft), and the traversing microphone was adjusted to be at ground level at a point 7.6 m (25 ft) from the base of the source, and to follow the reflected ray (angle of incidence $\alpha = 9.1^\circ$) out to 15 m from the source, with a positional accuracy of ± 10 mm. A fixed microphone was used to monitor the signal level.

3.5. Results

Data were taken at three frequencies: 1000, 1600, and 2000 Hz. Raw data and processed results are presented in Table 2. Two values are given for the microphone height at the position of the minimum: the first is a direct measurement, and the second is inferred from the horizontal distance and the known height vs. distance path followed by the traverse mechanism. It is not known which measurement is the more reliable; however, the discrepancy provides an estimate of the precision which may be inferred. The phase shift angles are computed from the average of the two height measurements, and rounded to the nearest 5° . The final two columns are results corrected for spherical wavefronts (see Section 8), and source directivity (2000 Hz only). These corrections affect the specific admittance ratio by less than 15% in each case.

The measured values of ΔL are as large as one can expect to measure. Thus, the deduced values of β may be higher than the true value, although the deduced values appear reasonable for unsealed asphalt.

It was not possible to run the traverse measurement on the sealed asphalt, since the advent of rain wetted the pavement at the time scheduled for this test, and scheduling limitations precluded waiting out the weather. Phase shift information from such a measurement would have been interesting; magnitude information would not be expected to reflect the actual very low specific admittance, due to the limitations in measuring ΔL discussed earlier.

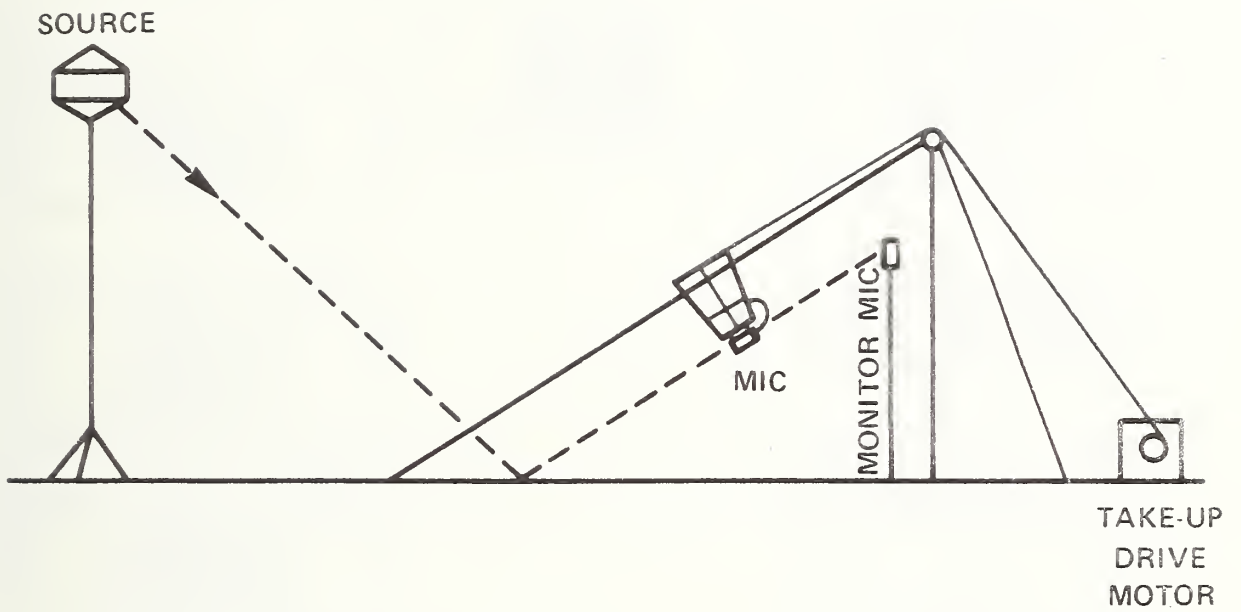


Figure 2. Sketch of Pure-Tone Traverse

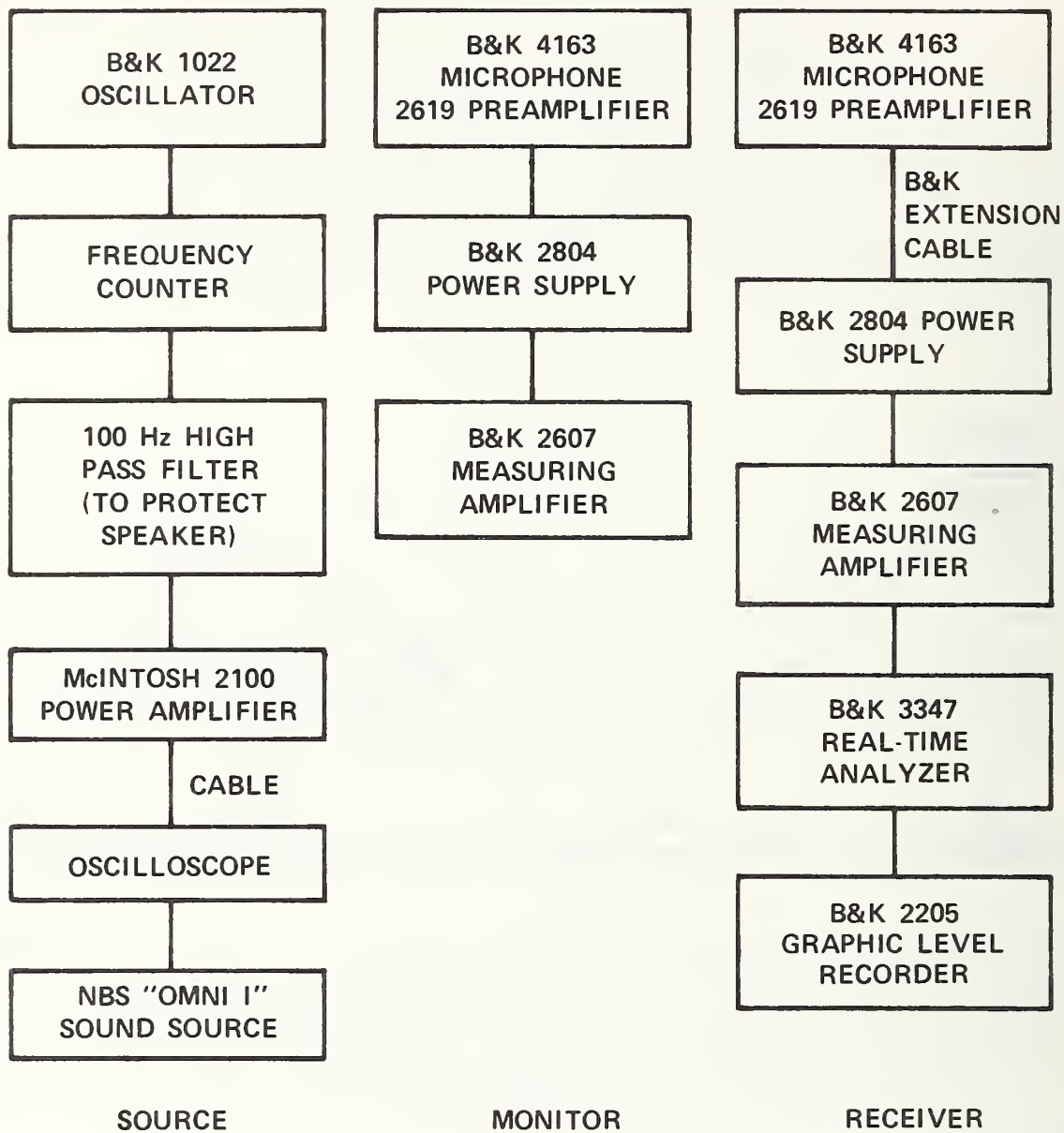


Figure 3. Block Diagram for Pure-Tone Traverse

Commercial instruments are identified in order adequately to specify the experimental procedure. In no case does such identification imply recommendation or endorsement by the National Bureau of Standards, nor does it imply that the equipment identified is necessarily the best available for the purpose.

Table 2. Pure-Tone Traverse Data

f (Hz)	r (m.)	h (m.)	ΔL (dB)	ϕ_r	$ C_r $	$ \beta $	arg β	Corrected $ \beta $ arg β (see text)
1000	11.706	.635	25	40°	.86	.059	-75°	.066
		.646						
1600	10.100	.384	23	20°	.84	.031	-60°	.034
		.398						
2000	9.808	.346	17	0°	.70	.028	0°	.025
		.352						

4. PULSE-ECHO MEASUREMENTS

4.1. Description of Experiment

In this technique a short pulse is emitted by the source, and the microphone receives and displays on an oscilloscope both the directly transmitted pulse and a reflected version. The reflected pulse is delayed and attenuated with respect to the direct pulse; its shape may be altered as well. The magnitude of the reflection coefficient is readily deduced from the attenuation of the reflected pulse:

$$|C_r| \frac{R_1}{R_2} = \frac{A_r}{A_d} = 10^{-\Delta L/20} \quad (4-1)$$

Here A_d and A_r represent the amplitudes of the direct and reflected signal pressures, ΔL is the difference in sound pressure levels, and R_1 and R_2 are the path lengths of the direct and reflected rays, respectively.

The phase shift is more difficult to determine, due in part to the fact that a short pulse cannot be a pure tone: the finite duration of the pulse means that more than one frequency must be present. Only if there were a phase shift at reflection which is proportional to frequency, would this be manifested as a simple time delay in the reflected pulse in addition to that due to the path length geometry. Phase shifts independent of frequency are not manifested as a uniform time translation of the waveform. Rather, the different frequency components are shifted by different times, resulting in distortion of the waveform. Such distortion is difficult to interpret.

Similar techniques have been cited in the literature [12-17]. In general, this previous work differed from the present experiment either in that normal incidence data was collected, or in that oblique incidence absorption data were obtained by comparing the test surface to a "hard" surface assumed to be perfectly reflecting. In this study it is the "hard" surface itself that is to be measured. Further, most of this previous work was performed indoors in a laboratory environment.

4.2. Advantages and Limitations

One advantage of the pulse-echo technique is the relative ease of relocating the source and microphone, enabling measurements to be conducted at different angles of incidence and different locations on the test pad. Frequency range is limited by the necessity for direct and reflected pulses to be non-overlapping. Thus the pulse width T_{pulse} must be smaller than the path length difference $\delta\tau$:

$$T_{\text{pulse}} < \delta\tau = (R_2 - R_1)/c \approx 2Hh/rc \quad (4-2)$$

(the last approximation is valid for glancing angles - see Figure 1).

Limitations in using this technique outdoors can be serious, however. Background noise even at 20 dB below the level of the signal makes precise reading of the amplitude using the oscilloscope very difficult. Furthermore, attempts to filter the received signal to lower the noise level result in broadening the pulse and causing the direct and reflected pulses to overlap. Also, phases are altered and waveforms distorted by the filter.

Further difficulties are caused by the wind. Wind turbulence causes rapid fluctuations in amplitude, time delay, and waveform, further complicating the reading of data. At a minimum, the measurement must be repeated a number of times and the results averaged; still the precision obtained in this study was limited.

Signal enhancement techniques, using a large number of recorded pulses, offer a means of substantially improving the signal to noise ratio, and hence the precision of the attenuation measurement. Further, the greater precision so obtained in the shape of the waveform would permit comparison of the measured shape with shapes predicted theoretically using various assumed values of the phase shift, and thus allow inferences to be drawn regarding the phase of the reflection coefficient. However, this approach involves a substantial increase in the complexity of data collection and analysis, and lies outside the scope of the present study.

Clearly, to obtain the attenuation $|C_r|$ from the amplitudes of the direct and reflected pulses, it is necessary for the source to radiate the same intensity in both the direct and reflected ray directions. A known amount of source directivity may be compensated for in the data reduction, but the accuracy of directivity corrections depends on the accuracy with which the source orientation is known.

4.3. Experiment

Pulse-echo measurements were taken at the Sandusky test site on August 26, 1976, before the asphalt had been sealed, and again on September 8, 1976, after sealing. Figure 1 depicts the geometry of the test; Figure 4 diagrams the electronic setup.

The lowest frequency obtainable in a pulse of a given duration is obtained from a single sinusoid (half a sine wave was ruled out because of loudspeaker constraints). Also, sinusoidal shape minimizes the high frequency content of the pulse. Thus a single sinusoid was chosen as the pulse shape. With the test geometries used, this allowed measurement down to 1000-2000 Hz as a lower frequency limit. Frequencies up to 4000 Hz were used. The sound source consisted of two Phillips 5060W8 speakers mounted on a cylinder, as described in Section 3.4.

The received signal was displayed on a dual-trace oscilloscope. The signal from the microphone was fed directly into one channel, and routed through a calibrated time delay circuit and a calibrated attenuator into the other channel. The time delay was adjusted to retard the direct pulse so that it would overlay the reflected pulse seen on the other channel. Then the attenuator was adjusted until the direct pulse amplitude was reduced to coincide, as well as possible, with that of the reflected pulse.

The time delay circuit was adjustable in 0.01 ms steps, the attenuator in steps of 0.1 dB. (Time delays for the September 8 measurements were determined

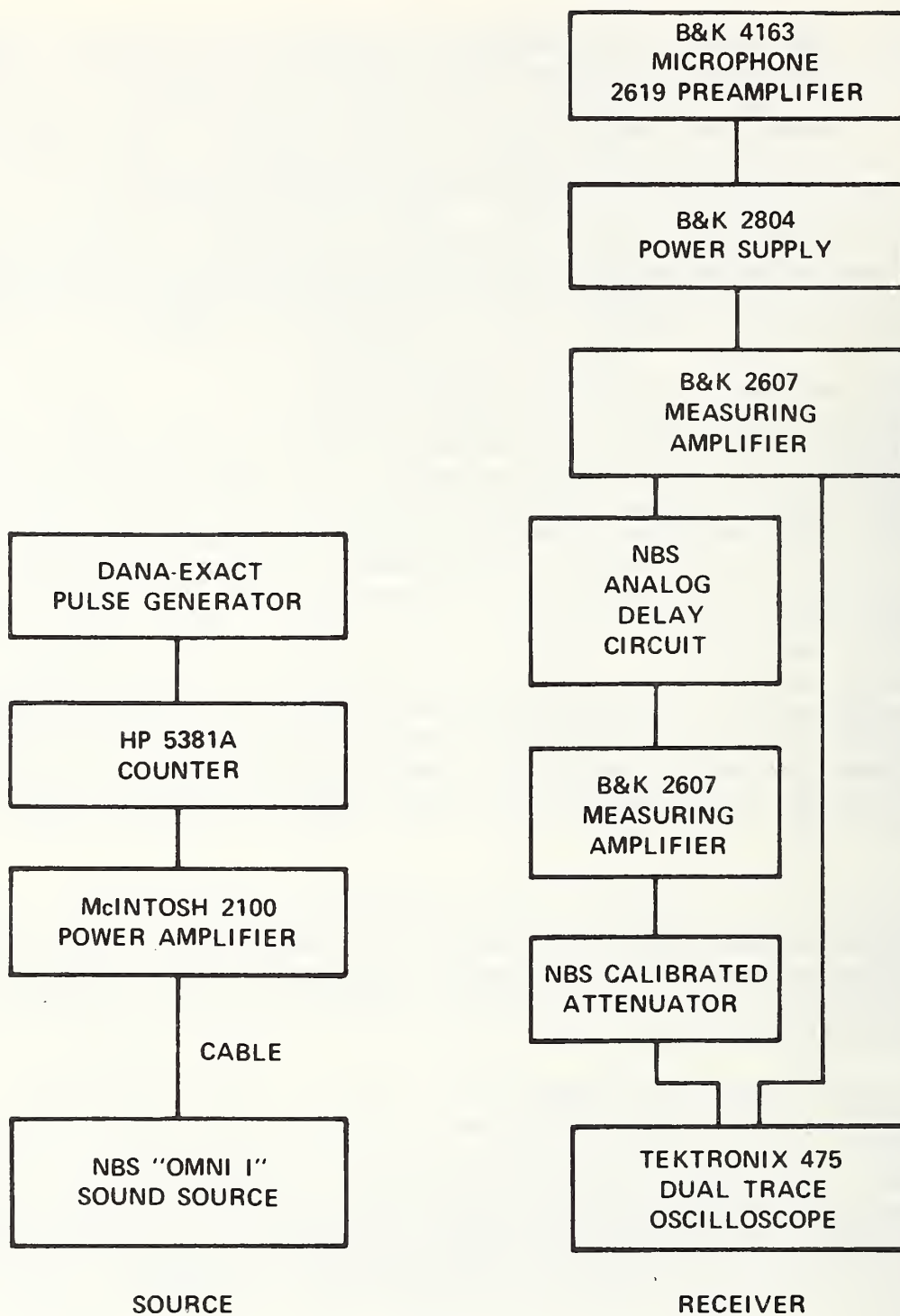


Figure 4. Block Diagram for Pulse-Echo

Commercial instruments are identified in order to adequately specify the experimental procedure. In no case does such identification imply recommendation or endorsement by the National Bureau of Standards, nor does it imply that the equipment identified is necessarily the best available for the purpose.

directly from the oscilloscope trace, because of a failure in the time delay circuit.)

4.4. Results

Results are presented in Table 3. Values of β at different frequencies were not averaged, since application of the F test for equality of the means (see e.g., Ref. [18]) indicated significant differences in mean values of β as a function of frequency, at the 95% confidence level.

The ratio of signal to noise varied between 10 and 20 dB, corresponding to amplitude ratios of 3:1 to 10:1. The signal cannot be filtered, for reasons discussed above; and the sound source was already being operated at maximum drive level. As a result of the large noise component, it was not possible to match the amplitudes of the direct and reflected waveforms to better than ± 0.5 dB (estimated), corresponding to errors in the deduced reflection coefficient of ± 0.05 . These errors are manifested in the large scatter of the deduced values of specific admittance ratio β (see Table 3). Negative values of $|\beta|$, in particular, clearly result from inaccuracies in the measurements propagating through the equations.

The noise is due both to ambient acoustic noise, and to air turbulence in the sound path. These problems could be minimized in the future by using a stronger signal source, by limiting observations to essentially windless conditions, or by averaging a very large number of received signal waveforms (signal enhancement).

As a further consequence of the noise, distortion in signal waveform, which would be expected from frequency-independent phase shifts at reflection, could not be observed. Thus no conclusions can be drawn about these phase shifts.

The time difference between direct and reflected pulses could be measured quite accurately (estimated error of ± 0.02 ms), and results agree with values predicted from the geometry alone. Thus, there was no evidence for reflection phase shifts proportional to frequency, which would be manifested as additional time delays.

Corrections for wind and temperature gradients were not applied, since known measurement uncertainties alone make the pulse-echo data unreliable. Corrections for spherical wavefronts would be even smaller. Source directivity is believed to be a serious problem, particularly at the higher frequencies. Directivity data at 3-4 kHz were not available, but the known directivity at 2.5 kHz indicates that uncertainties in source alignment, estimated at $\pm 3^\circ$, would make futile any attempt to correct the measurements by measuring the source directivity a posteriori.

Table 3. Pulse-Echo Data

Run	Angle of Incidence α (deg.)	Frequency (kHz)	Measured Attenuation ΔL (dB)	Refl. Coeff. $ C_r $	Specific Admittance Ratio $ \beta $	$\delta\tau_{meas}$ (ms)	$\delta\tau_{comp}$ (ms)
UNSEALED ASPHALT							
1	17.6	4	2.5	.79	.035	2.28	2.21
		3	2.0	.83	.028	2.28	2.21
		2	1.8	.85	.025	2.26	2.21
		1.6	1.3	.90	.016	2.26	2.21
		1	0.3	1.01	-.002	2.26	2.21
2	13.5	4	4.3	.62	.055	1.18	1.12
		3	3.4	.69	.043	1.18	1.12
		2	1.7	.84	.020	1.18	1.12
		1.6	1.0	.91	.011	1.18	1.12
		1	0.8	.93	.008	1.18	1.12
3	9.1	4	4.3	.62	.037	.60	.57
		3	3.2	.70	.028	.60	.57
		2	0.3	.98	.002	.60	.57
Average (std dev)		4			.042(.011)		
		3			.033(.009)		
		2			.016(.012)		
		1.6			.014(.004)		
		1			.003(.007)		
SEALED ASPHALT							
4	13.5	4	1.4	.87	.016	1.04	1.12
		3	0.9	.92	.010	1.04	1.12
		2	0.1	1.01	-.001	1.04	1.12
		1.6	0.2	1.00	.000	1.04	1.12
5	13.5	4	1.8	.83	.022	1.08	1.12
		3	0.9	.93	.008	1.08	1.12
		2	-0.2	1.05	-.006	1.08	1.12
		1.6	-0.2	1.05	-.006	1.08	1.12
6	12.6	4	1.2	.89	.013	-	1.05
		3	0.5	.97	.003	-	1.05
		2	0.0	1.02	-.002	-	1.05
		1.6	0.0	1.02	-.002	-	1.05

Run	Angle of Incidence α (deg.)	Frequency (kHz)	Measured Attenuation ΔL (dB)	Refl. Coeff. $ C_r $	Specific Admittance Ratio $ \beta $	$\delta\tau_{\text{meas}}$ (ms)	$\delta\tau_{\text{comp}}$ (ms)
7	12.6	4	0.1	1.01	-.001	-	1.05
		3	0.1	1.01	-.001	-	1.05
		2	0.0	1.02	-.002	-	1.05
		1.6	0.0	1.02	-.002	-	1.05
8	9.6	4	0.6	.94	.005	.72	.80
		3	1.2	.88	.011	.73	.80
		2	0.6	.94	.005	.75	.80
9	9.6	4	0.8	.92	.007	.77	.80
		3	0.4	.97	.003	.76	.80
		2	0.4	.97	.003	.75	.80
10	12.7	4	1.5	.86	.017	1.62	1.59
		3	0.8	.93	.008	1.62	1.59
		2	0.6	.95	.006	1.62	1.59
		1.6	1.2	.89	.013	1.60	1.59
		1	2.3	.79	.026	1.60	1.59
11	17.6	4	2.0	.83	.028	2.20	2.21
		3	1.1	.92	.013	2.20	2.21
		2	1.0	.93	.011	2.20	2.21
		1.6	0.9	.94	.009	2.20	2.21
		1	0.2	1.02	-.003	2.25	2.21
12	16.5	4	1.3	.90	.015	2.10	2.06
		3	1.1	.92	.012	2.10	2.06
		2	0.6	.98	.003	2.10	2.06
		1.6	0.3	1.01	-.001	2.10	2.06
		1	0.1	1.04	-.006	2.10	2.06
Average (std dev)		4			.014(.009)		
		3			.007(.005)		
		2			.002(.005)		
		1.6			.002(.007)		
		1			.006(.018)		

5. Broad-Band Cross-Correlation

5.1. Description of Technique

5.1.1. Data Collection

This technique also uses the glancing-angle geometry depicted in Fig. 1. The source in this case emits broad-band noise, and a second microphone is introduced very near the source. Signals received by both the near-field and far-field microphones are recorded simultaneously on a multichannel tape recorder.

Subsequently, the two recorded signals are processed using a cross-correlation analyzer. This is a microcomputer specifically designed to compute the cross-correlation function $R_{12}(\tau)$ of two time-varying analog signals $p_1(t)$ and $p_2(t)$. R_{12} is defined by

$$R_{12}(\tau) = \lim_{T \rightarrow \infty} \frac{1}{T} \int_0^T p_1(t) p_2(t+\tau) dt. \quad (5-1)$$

(In practice, of course, T does not go to infinity, but it must be chosen large enough that the error in R_{12} due to finite T is within bounds set by the experimenter. If $p_2 = p_1$, Eq. (5-1) defines the auto-correlation. A detailed discussion of correlation functions, and also of cross spectral functions, may be found (e.g.) in Bendat and Piersol[19]. The output of the correlation analyzer may be used to drive an x-y plotter to produce a correlogram, a graph of R_{12} versus τ (Fig. 5).

Correlation techniques have been used by others to measure absorption or specific impedance (see e.g. [20,21,22]). In these earlier experiments, normal incidence measurements were performed. In many cases, the microphone signal was correlated with the electrical signal input into the speaker. Speaker response distorts the correlogram, and absorption must then be determined by comparison with data from a "perfectly reflecting" surface. In the present study it is the impedance of the "perfectly reflecting surface" itself which is to be measured. Thus a near-field microphone was introduced to eliminate the effect of speaker response.

It is also possible to extract impedance data from the autocorrelation of the far-field microphone compared to the autocorrelation of the near-field signal. For low values of β , this alternative procedure provides less precision in β than the cross-correlation technique studied here.

5.1.2. Correlogram Features

A typical correlogram obtained during this study is reproduced in Figure 5. Such correlograms reveal certain information about the propagation paths of the signal. For example, two prominent peaks may be noted, representing the direct and reflected signals respectively. Since the far-field microphone receives the

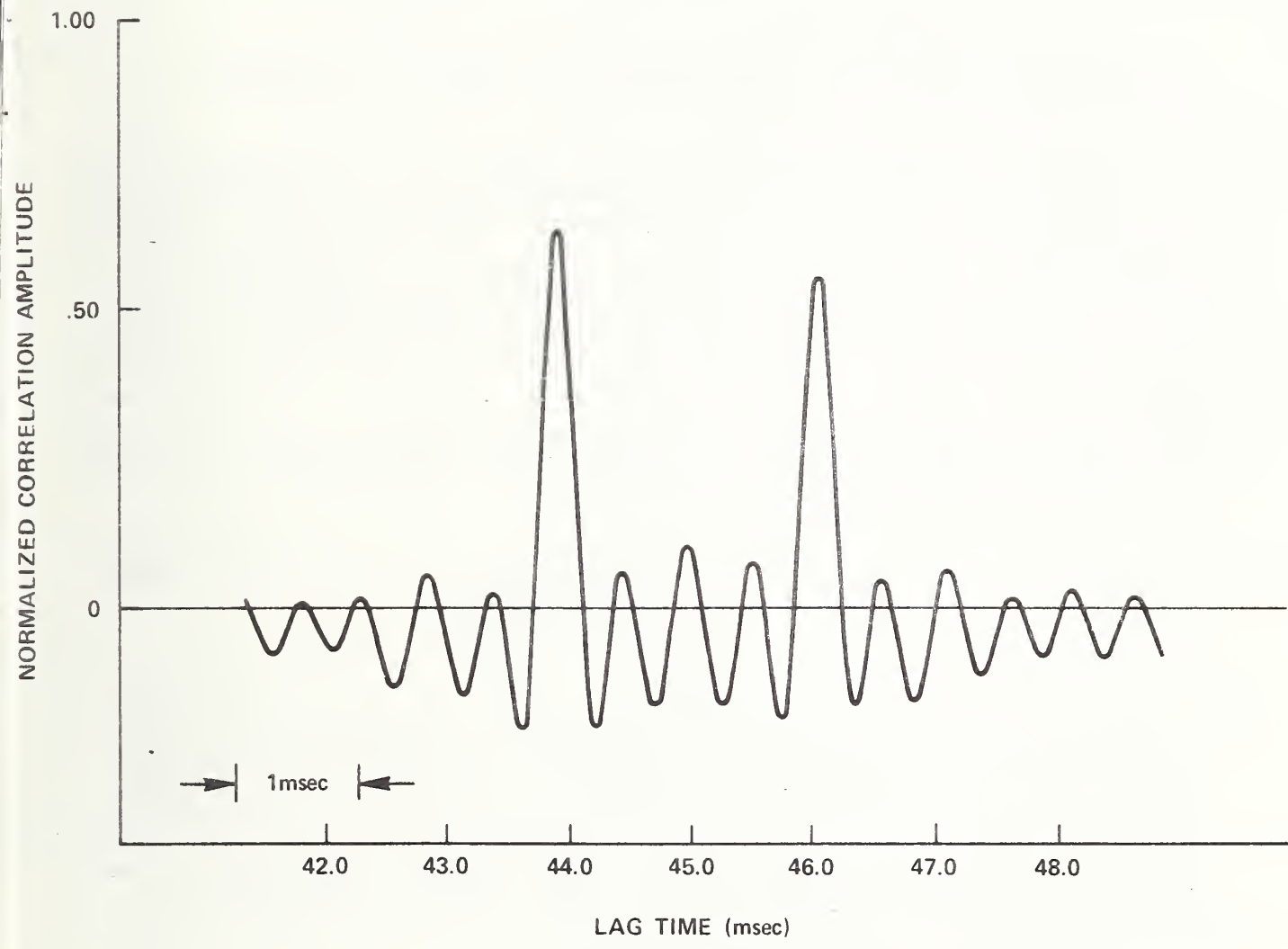


Figure 5. Example of Cross-Correlogram

same (direct) signal as the near-field microphone, but delayed by the propagation time Δ , there is a strong correlation between the two received signals when a time lag of Δ is introduced into the near-field signal. Thus, $R_{12}(\tau)$ exhibits a peak at $\tau = \Delta$. Similarly, the reflected signal introduces a second peak. Since the reflected path is longer by δ than the direct path, the second peak appears at a longer time delay $\Delta + \delta$. Further, since the reflected signal is attenuated, the correlation is not quite as strong and the second peak is not as high.

5.1.3. Extraction of Reflection Coefficient

It will be assumed in the following analysis that C_r is independent of frequency. Removal of this restriction will be discussed later.

If the sound source were a truly random signal, i.e., infinite bandwidth white noise, then the ratio of the amplitudes of the two correlogram peaks would equal $|C_r| R_1/R_2$, the magnitude of the reflection coefficient times a spherical divergence factor, at least for real values of C_r . (The assumption $\phi_r = 0$ is not unreasonable - see below.) In practice, of course, the loudspeaker is limited in frequency response at both high and low frequencies. The use of band-limited white noise introduces oscillations in the correlogram, also seen in Figure 5. The correlation functions for band-limited white noise, for the experimental geometry under study, are derived in Appendix C. A further consequence of the oscillations introduced by the finite bandwidth of the signal is that the oscillations resulting from one peak add to the amplitude of the other peak. Thus the observed amplitude ratio is in fact

$$\frac{A_2}{A_1} = \frac{r_{ss}(\delta) + |C_r| R_1/R_2}{1 + r_{ss}(\delta) |C_r| R_1/R_2}, \quad (5-2)$$

as derived in Appendix C, and not simply $|C_r| R_1/R_2$. Here $r_{ss}(\delta)$ is the source(near-field) autocorrelation function at $\tau = \delta$, normalized by the mean squared value of the signal. In the absence of a reflected wave, the cross-correlation would be a replica of the source autocorrelation, shifted by the propagation time Δ , and possibly attenuated in the vicinity of the peak, due to the presence of ambient background noise. Thus it is not surprising that the actual cross-correlation behaves like the superposition of two source autocorrelations.

As usual, β is obtained from C_r using Eq. (3-2).

5.2. Advantages and Limitations

There are a number of advantages to this broad-band cross-correlation technique. Since several minutes of recorded data are used to perform the correlation, the result is an average of air turbulence evolving over a period of time, and is not sensitive to instantaneous fluctuations in the ray paths.

The gathering of data is relatively simple, and long samples may be taken, using a number of different source-receiver geometries, quite inexpensively. It is however necessary to measure the source and receiver positions accurately (± 1 cm for all dimensions has been required in this study, corresponding to a precision of $\pm .001$ in β).

Ambient noise and instrument noise are no great problem. Noise generally does not cross-correlate with the same delay time as the signal. The principal effect of a moderate amount of noise is to lower the correlation amplitudes by a constant factor, which is eliminated in taking the ratio of two peaks.

Additional information is contained in the correlograms. Steady wind causes changes in the signal propagation time; thus, the location of the first peak is a very sensitive measure of the average wind component in the direction of propagation. On the other hand, the propagation time difference between the two peaks is independent of uniform wind, but it is affected by wind gradients, as discussed in section 7. By setting up the experiment to record simultaneously signals propagating in two opposite directions, effects of horizontal wind (which are positive in one direction and negative in the other) can easily be separated from other factors such as temperature gradients uniform over the test pad, which have the same effect regardless of the direction of propagation.

Additional features, such as the relative amplitudes and spacing of the smaller peaks, are affected by the phase of the reflection coefficient, and by its frequency dependence. These effects can be studied by mathematical modeling: deriving analytic expressions for the cross-correlation functions using different values of the parameters (e.g., ϕ_r), and plotting the resulting correlograms for comparison with field data.

Some assumption about ϕ_r , the phase of the reflection coefficient, is necessary to infer $|C_r|$ from the correlogram peak heights. Eq. (5-2) above was derived assuming $\phi_r = 0$. For a very hard locally reacting surface and typical source emission measurement geometries, ϕ_r is quite small even for a large value of $\arg \beta$, as a result of Eq. (1-2). Thus the assumption $\phi_r = 0$ is reasonable to use during data reduction. (Conversely, the phase of β cannot be accurately determined from a measured ϕ_r .)

A difficulty in using this technique is the need for a source which is omnidirectional over the entire frequency range being used, at least within the angles spanned by the direct and reflected ray paths. The difficulty of meeting this requirement is increased when measuring in two directions at once. Although in principle a known source directivity might be accounted for, in practice this is limited both by inaccuracy in orienting the source, and by the variation of directivity with frequency. In addition, microphone directivity effects must be accounted for to obtain the greatest possible precision.

Frequency dependence of β raises many questions. It is likely that a study of cross-spectral density functions - the Fourier transform of cross-correlation

functions - would provide information on frequency dependence (see e.g., Ref 23). Computer modeling, including frequency-dependent parameters in the model, would also provide such information. Both of these avenues lie outside the scope of this study. It should be noted that in the absence of spectral decomposition, it is only a frequency-averaged impedance that is measured, and not the impedance as technically defined for a single frequency.

An additional difficulty in using this technique is the requirement for test source emission which is "white" within its frequency range, i.e., radiating equal energy per unit bandwidth. The equal energy requirement was imposed to minimize the need for detailed frequency studies, to achieve the highest resolution consistent with the usable bandwidth, and to permit analytic solutions of the mathematical model.

An alternative of combining a broad-band cross-correlation technique with the impedance tube apparatus, as described in Ref. [20], would eliminate wind problems. However, the normal reflection coefficient is so much closer to 1 than the glancing angle coefficient (at least for a locally reacting surface) that much greater precision would be required of the measurements, to achieve comparable precision in the inferred β . It is not known whether the necessary precision could be achieved.

5.3. Experiment

5.3.1. Configuration

Broad-band recordings were made at the Sandusky test pad on September 9, 1976, after the asphalt had been sealed. (Good data could not be collected on the previous survey - before sealing - because the original sound source did not have sufficient power-handling capability relative to the ambient noise conditions which were found at the site.)

The ray diagram of Fig. 1 is applicable to this experiment. Source/microphone geometry is indicated in Figs. 6 and 7. Two near-field and eight far-field microphones were recorded simultaneously, providing data for a number of source/receiver geometries, including simultaneous upwind and downwind measurements. A block diagram of the test setup is presented in Fig. 8. The sound source for this measurement used two KEF B-110 speakers, one at each end of a plastic cylinder 75 mm long and 200 mm in diameter. Although similar to the original sound source which used Phillips speakers, the second source proved to be somewhat more directional. A spectrum shaper between the noise generator and the speakers was adjusted so that the sound radiated by the speakers was as nearly as possible "white" in the frequency band 100-2500 Hz, and rolled off sharply outside this band. At 15.2 m (50 ft.), the overall sound pressure level of the band-limited signal (100 Hz - 2500 Hz) was about 70 dB. Flatness in frequency as measured using a 5 Hz bandwidth narrow-band analysis, was achieved to within +4 dB.

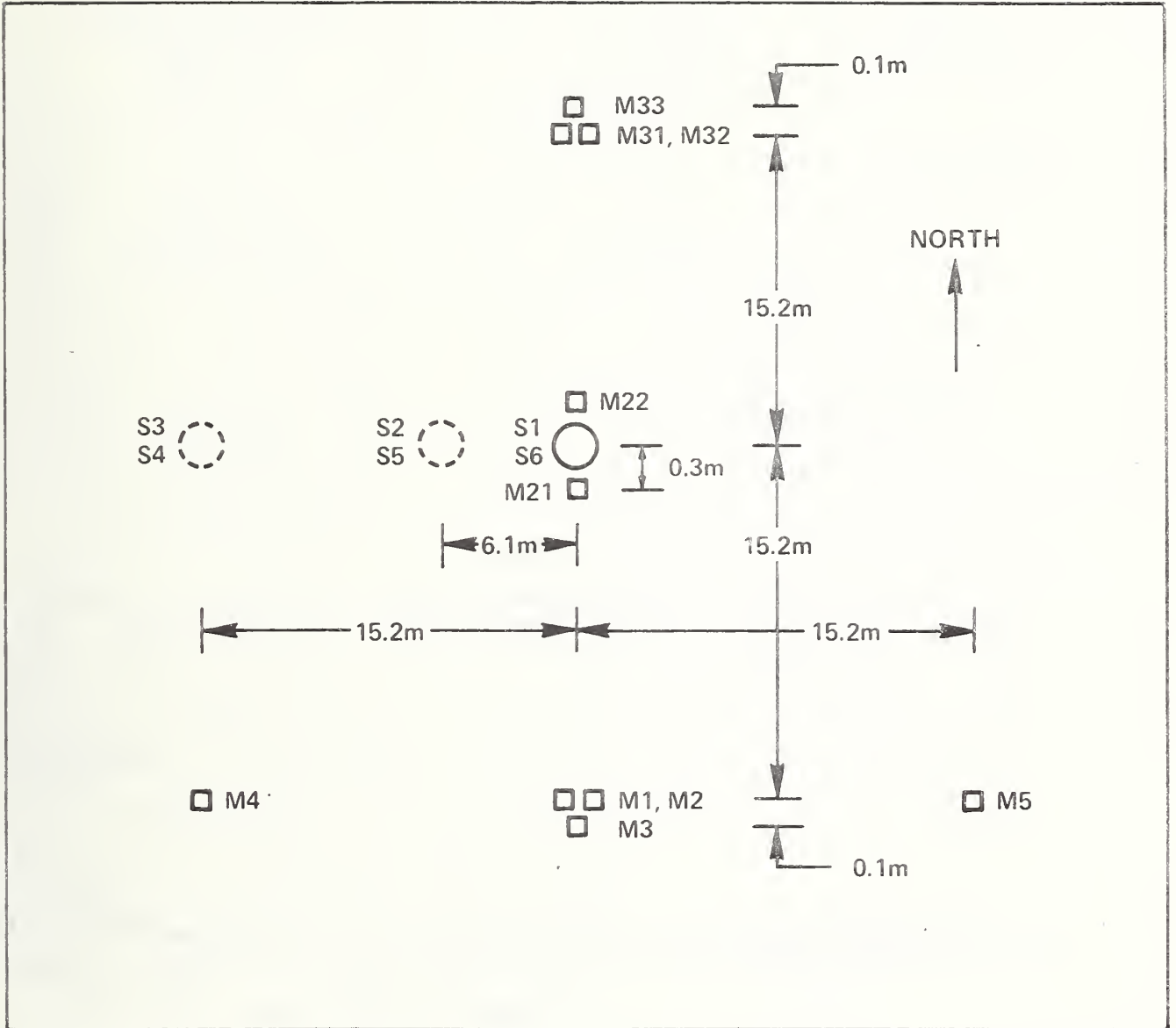


Figure 6. Source and Microphone Layout - Plan View
 Source positions (circles) and microphone positions (squares) are numbered for identification with the corresponding positions in Table 4.

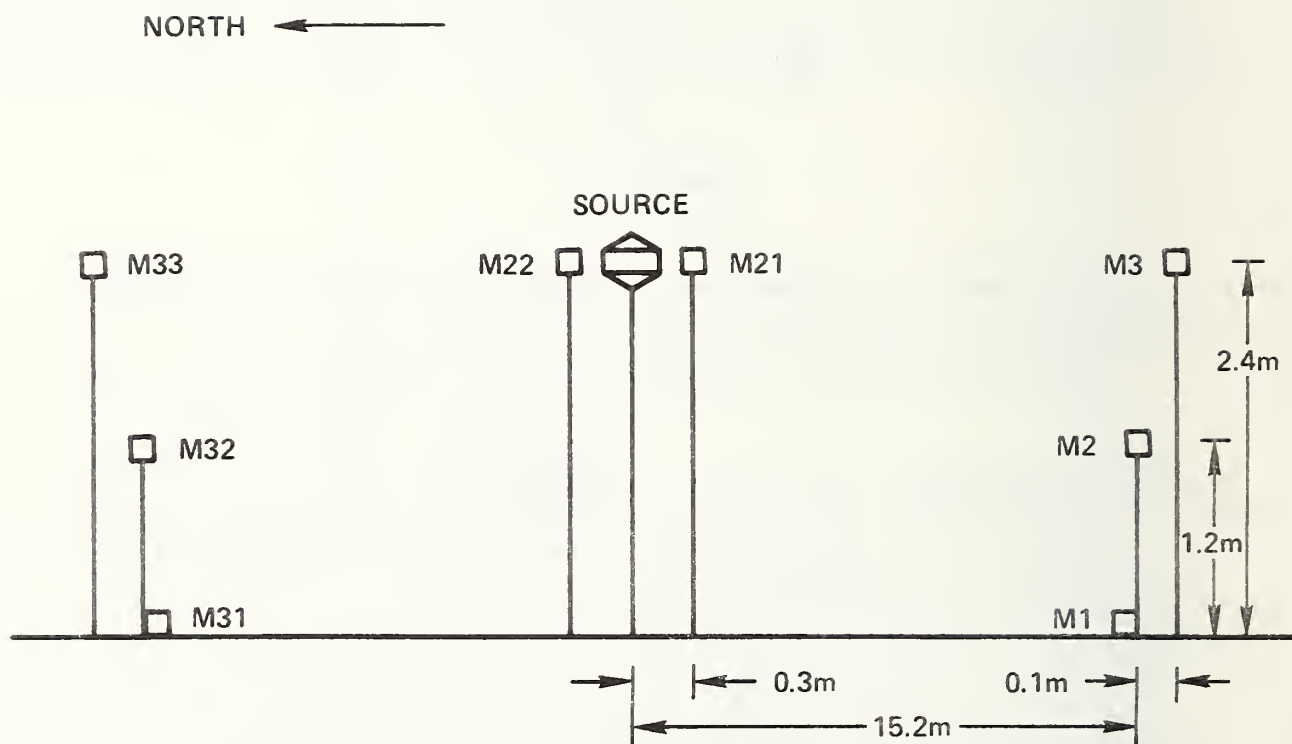


Figure 7. Source and Microphone Layout - Elevation
 Source positions (circles) and microphone positions (squares) are numbered for identification with the corresponding positions in Table 4.

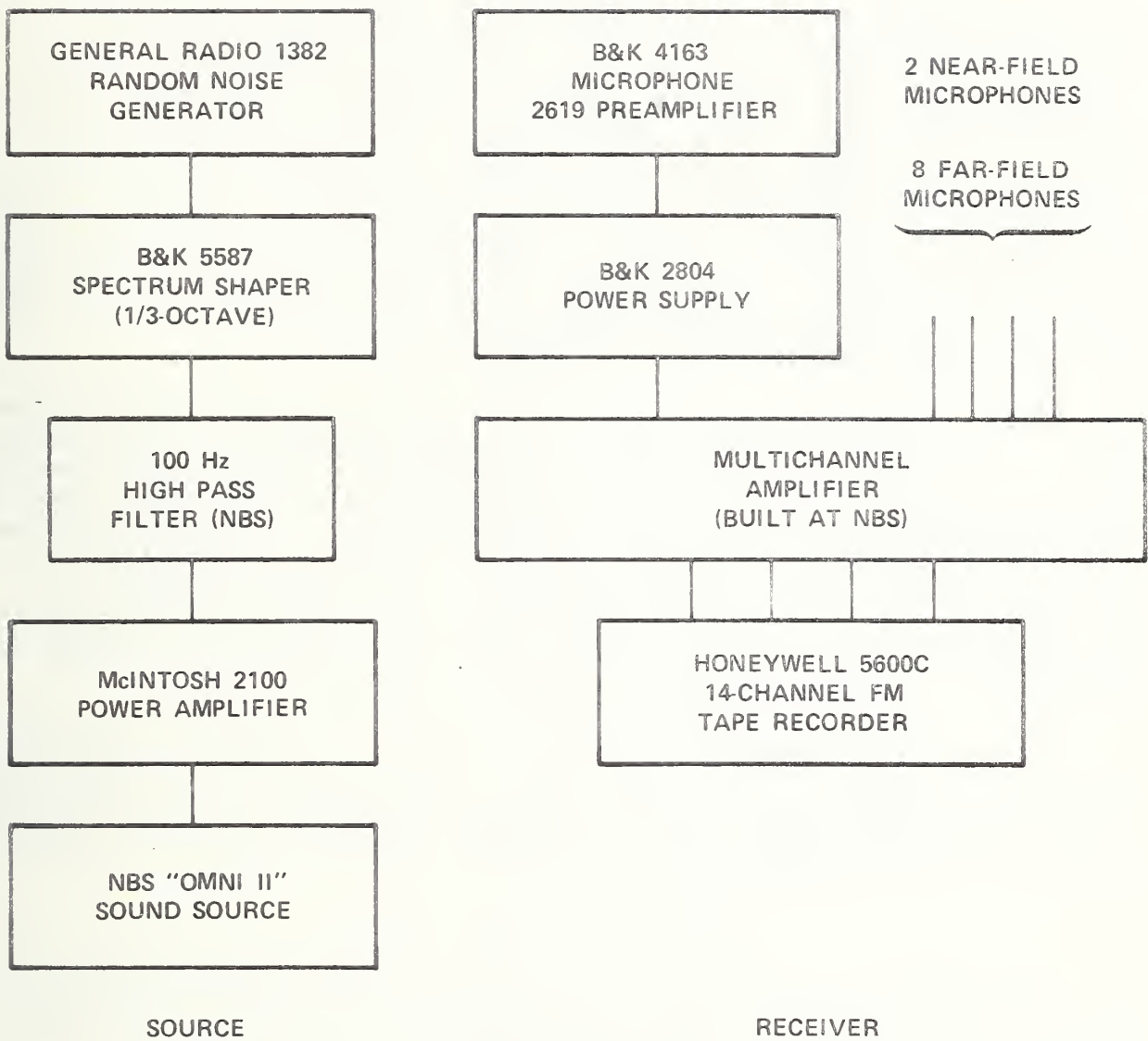


Figure 8. Block Diagram for Broad-Band Cross-Correlation - Data Collection

Commercial instruments are identified in order adequately to specify the experimental procedure. In no case does such identification imply recommendation or endorsement by the National Bureau of Standards, nor does it imply that the equipment identified is necessarily the best available for the purpose.

5.3.2. Locations of Source and Microphones

Nine positions of the source were recorded: three with the source 2.4 m (8 ft) above the ground, three at 1.2 m (4 ft), and three at ground level. The eight microphone positions include two at 2.4 m (8 ft), four at 1.2 m (4 ft), and two at ground level (see Figs. 6 and 7). The elevated microphones were oriented so that the normal to the diaphragm was vertical; the ground level microphones were oriented so that the direct ray from the source was at grazing incidence. Data obtained from the ground-level locations can be useful for validation of detailed models, including wind and temperature effects. Such detailed modeling, however, is outside the scope of this study. Measurement of the reflection coefficient using the two main peaks in the correlogram, as described above, requires that both source and microphone be above ground level. Thus six elevated source positions and six elevated microphone positions provided thirty-six measurements for the present analysis.

Thirty of these measurements were used to compute average values of the specific acoustic admittance ratio β , and standard deviations of the measured β . The six configurations with the smallest propagation time difference δ were not included in these averages. At these small values of δ , less than 0.5 ms, the source autocorrelation $r(\delta)$ varies rapidly and may be large; further, accurate source autocorrelograms were not obtained for all source positions. The anticipated errors in β (and in peak spacing δ) introduced by these uncertainties in $r(\delta)$ were much greater than for the remaining thirty measurements. (Had the other six measurements been included, the average β would not have changed, but the scatter would have been increased.)

It is implicitly assumed that the admittance of the asphalt is the same from point to point, and that the standard deviations from the 30 measurements reflect measurement imprecision and not actual variations in the surface. It is hoped that this assumption will be validated or rejected by future studies in which the sources of error are more closely controlled.

5.4. Initial Data Reduction

Data reduction (correlation) was carried out using a Saicor SAI-43A 400 point correlation analyzer, in the configuration shown in Fig. 9. Initially the correlation was carried out using 0.1 ms resolution [i.e., $R(\tau)$ was computed at increments of 0.1 ms in τ] and did not require the analog delay circuit shown in Fig. 9.

Correlation amplitudes obtained from this analysis were used to compute values of β , using Eqs. (5-2) and (5-3). The average value of β based on thirty source-receiver geometries was $\beta = .010$. However, these data showed a great deal of scatter, as reflected in the standard deviation of the thirty measurements of β , $\sigma = .008$.

Additionally, the measured values of C_r were plotted as a function of $1/\sin \alpha$. (These plots are not reproduced here.) Ideally, the plotted points would lie on a straight line with a slope of 2β . It is believed, however,

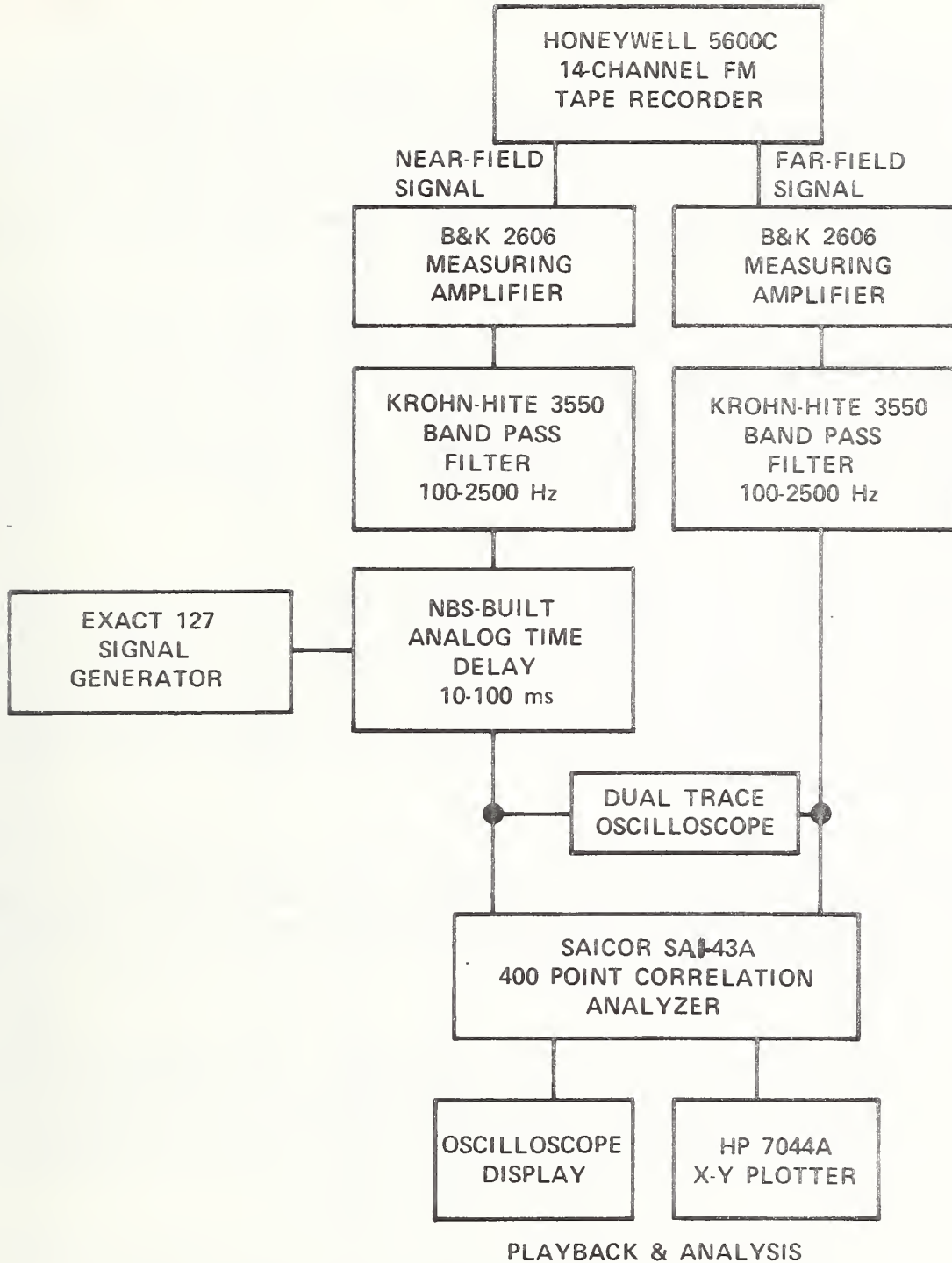


Figure 9. Block Diagram for Broad-Band Cross-Correlation Data Reduction

Commercial instruments are identified in order adequately to specify the experimental procedure. In no case does such identification imply recommendation or endorsement by the National Bureau of Standards, nor does it imply that the equipment identified is necessarily the best available for the purpose.

that the measured relationship between C_r and $1/\sin \alpha$ could be nonlinear, or linear but with a non-zero intercept -- due perhaps to temperature gradients, position measurement errors, or inapplicability of the point impedance model. In this case, the points might cluster closely around a curved line, even though the scatter of β 's deduced from the straight line model was large. Such was not the case, however: the plot of C_r vs. $1/\sin \alpha$ showed a great deal of scatter, which appeared to be consistent with the scatter about the straight line model.

It was, however, noted that the peaks displayed on the correlograms were spikey, not smooth, and it was suspected that perhaps with 0.1 ms resolution the true peaks were being missed, resulting in errors in the measured amplitudes. By computing a correlogram based on an analytic model, using a high-speed digital computer, this was demonstrated to be the case. Limiting the resolution to 0.1 ms resulted in amplitudes being underestimated by varying amounts, often several percent, leading to substantial errors in the computed values of β .

5.5. Final Data Reduction and Results

The entire analysis was therefore rerun with a resolution of 0.02 ms. At this resolution, errors were expected to be less than 0.3%, less than the 0.5% errors inherent in the x-y plotter and the reading of the correlograms. These errors, in turn, when propagated through the data reduction equations, would lead to worst-case uncertainties in the value of β of about .002. This was felt to be a useful and realistic target; useful in that effects of uncertainties in β on source emission measurements could then be reduced to within a few tenths of a dB (see Section 9).

Results of the analysis using 0.02 ms resolution are presented in Table 4. The average specific admittance ratio, based on thirty measurements, is $\beta = .007$; the standard deviation of the thirty measurements of β is $\sigma = .004$. These results clearly reflect a reduction in the scatter of data. Further, plots of C_r vs. $1/\sin \alpha$ show a similar reduction in scatter; however, substantial scatter remains.

A number of possible sources of error were considered. These can be divided into measurement errors, errors in the model, and simplifications used in applying the model. The first group includes errors in correlogram resolution - as noted above these are believed to affect β by less than .002 - and errors in position measurement, believed to be very small (see below).

5.6. Analysis of Delay Times

To verify the accuracy of the position measurements, measured values of the propagation time difference δ_{meas} were compared with computed values $\delta_{\text{comp}} = 2Hh/r'c$, where $r' = r[1 + (H^2 + h^2)/2r^2]$. Since $\delta \approx 2Hh/rc$, relative errors in position (e.g., $\Delta H/H$) translate into relative errors in δ (i.e., errors in $(\delta_{\text{meas}} - \delta_{\text{comp}})/\delta$). Statistics of the relative errors were therefore examined. The average of thirty relative errors was -0.8%, with a standard deviation of 2.9% (of the typical δ of 1-2 ms).

The non-zero average of the thirty errors could be attributed to a corresponding error in average sound speed c , due to an uncertainty in temperature

Table 4. Broad-Band Cross-Correlation Data

Source Pos.	Mic. Pos.	H (m)	h (m)	r (m)	α (deg)	δ_{meas} (ms)	A_1	A_2	$r_{\text{SS}}(\delta)$	$ C_r $	β^0	β^w
S1	M2	2.4	1.2	15.2	13.5	1.12	.72	.69	.09	.974	.003	.002
	M3		2.4	15.3	17.6	2.18	.68	.57	-.02	.885	.018	.017
	M32		1.2	15.2	13.5	1.12	.70	.68	.09	.990	.001	.002
	M33		2.4	15.3	17.6	2.22	.65	.57	-.02	.925	.012	.013
	M4		1.2	21.5	9.6	.78	.64	.55	-.14	.904	.008	.007
	M5		1.2	21.5	9.6	.78	.63	.54	-.14	.902	.009	.007
S2	M2	2.4	1.2	16.4	12.6	1.07	.65	.63	.11	.985	.002	.000
	M3		2.4	16.5	16.5	2.06	.65	.55	-.05	.896	.016	.014
	M32		1.2	16.4	12.6	1.07	.68	.68	.11	1.025	-.003	-.002
	M33		2.4	16.5	16.5	2.10	.60	.53	-.03	.927	.011	.012
	M4		1.2	17.8	11.6	1.00	.69	.63	.06	.922	.008	.007
	M5		1.2	26.2	7.9	.61	.65	.58	.07	.867	.009	.008
S3	M2	2.4	1.2	21.5	9.6	.78	.62	.52	-.14	.889	.010	.008
	M3		2.4	21.6	12.7	1.59	.66	.61	.06	.938	.007	.006
	M32		1.2	21.5	9.6	.82	.63	.55	-.15	.917	.007	.009
	M33		2.4	21.6	12.7	1.60	.62	.58	.07	.949	.006	.007
	M4		1.2	15.2	13.5	1.09	.70	.64	.11	.920	.010	.011
	M5		1.2	34.1	6.1	.51	.63	.57	.10	.890	.006	.005
S4	M2	1.2	1.2	21.5	6.5	.43	.53	.52	.02	-	-	-
	M3		2.4	21.6	9.6	.76	.56	.51	-.10	.940	.005	.004
	M32		1.2	21.5	6.5	.44	.50	.53	.03	-	-	-
	M33		2.4	21.6	9.6	.80	.51	.47	-.09	.948	.004	.006
	M4		1.2	15.2	9.1	.53	.67	.60	.10	.886	.010	.007
	M5		1.2	34.1	5.1	.20	-	-	-	-	-	-
S5	M2	1.2	1.2	16.4	8.5	.53	.69	.64	.10	.923	.006	.004
	M3		2.4	16.5	12.5	1.02	.69	.64	.03	.946	.006	.005
	M32		1.2	16.4	8.5	.55	.69	.64	.09	.925	.006	.008
	M33		2.4	16.5	12.5	1.07	.67	.62	.05	.939	.007	.008
	M4		1.2	17.8	7.8	.49	.66	.61	.10	.916	.006	.004
	M5		1.2	26.2	5.3	.24	.60	.48	-.11	-	-	-
S6	M2	1.2	1.2	15.2	9.1	.54	.70	.62	.09	.876	.010	.008
	M3		2.4	15.3	13.4	1.08	.61	.54	.06	.893	.013	.012
	M32		1.2	15.2	9.1	.56	.68	.63	.08	.926	.006	.008
	M33		2.4	15.3	13.4	1.12	.65	.60	.06	.945	.007	.008
	M4		1.2	21.5	6.5	.33	.54	.48	-.20	-	-	-
	M5		1.2	21.5	6.5	.42	.59	.51	.00	-	-	-

NOTE: β^w represents inferred values of β after including the effects of wind.
 β^0 does not account for wind effects.

of 0.5 °C. However, c had been computed from the positions of the first correlogram peak. Further examination showed systematic differences in "northerly" vs. "southerly" measurements. These differences were attributed to wind gradients, which are discussed in detail in Section 7. Corrections to δ due to wind gradients are also derived there. These corrections were applied, assuming a 1 m/s wind speed (at 1.2 m height) from the south (reasons for this choice are discussed later).

After applying the wind corrections, the averaged errors in δ were -0.1%; however the standard deviation was still a comparatively large 2.7% (0.004 ms). By grouping the measurements according to source position and (separately) according to microphone position (Table 5), any error in measurement of H or h would show up as a systematic error in δ in one group compared to the other groups. Such between group variations were not statistically significant, and it is believed that accuracy in H and h is confirmed to within ± 1 cm. Effects on δ of similar errors in r are much smaller; effects on β would also be small (the importance of accuracy in r is its use in deriving wind and temperature information from first peak positions - see below).

5.7. Sources of Error

Thus the measurement errors - peak height and source-receiver positions - do not account for the observed scatter in β . However, the assumptions and simplifications used in reducing the data may well account for these discrepancies. These simplifications included ignoring wind and temperature gradients, assuming zero phase shift ($\phi_r = 0$), assuming C_r is independent of frequency, assuming uniform source directivity, and ignoring spatial variations of β and deviations of the asphalt surface from flatness. Also, the point impedance model itself may prove inadequate.

A number of these simplifications were removed by further study, and these will be discussed below because of their applicability to future measurements. In fact, the source directivity was shown to be a serious problem, sufficient by itself to account for all the observed data scatter. Differences in radiated intensity of direct and reflected rays were several decibels for frequencies above 2000 Hz, for some of the geometries. Even averaged over all frequencies, differences of more than 1 decibel must be expected. Although known directivity could have been accounted for in the model, the source orientation was not known with sufficient accuracy to obtain any meaningful improvement. It may be noted that the inclusion of directivity information tends to lower the deduced values of β , for this particular experiment.

Microphone directivity also needs to be considered in the future assuming source directionality is reduced. It is estimated that the difference in microphone sensitivity to the direct vs. the reflected rays may be as high as 0.5 dB at 2500 Hz, or perhaps 0.2 dB overall, for the particular microphones used, oriented vertically as described.

The effect of assuming $\phi_r = 0$ was studied by generating correlograms using the analytic expressions derived in Appendix C. Figure 10 shows three such correlograms, for $\phi_r = 0, -10^\circ,$ and -70° . Note the changes in the "fine structure" of the correlogram, i.e., in the smaller features, resulting from a 10° change in ϕ_r . Deviations of 10° are readily detected, and one may conclude that $\phi_r = 0 \pm 10^\circ$. (It is noted that for the locally reacting point impedance model, $C_r = (\sin \alpha - \beta) / (\sin \alpha + \beta)$, so that given the geometry of the experiment and assuming $|\beta| < .01$, the predicted value of ϕ_r must be less than 10° regardless of the phase of β .)

Table 5. Measured vs. Predicted Propagation Time Differences

$100 (\delta_{\text{meas}} - \delta_{\text{pred}}) / \delta$, percent, after wind corrections

microphone position

Source Position	2	3	4	5	32	33	row average	Standard error of mean, = std dev/ \sqrt{n}
1	+2	0.0	0	0	-2	-1.0	-0.2	0.5
2	+4	+1.5	+5	-5	0	+0.5	+1.0	1.4
3	0	+2.0	-1	+4	0	-1.5	+0.6	0.8
4	-	-3	-4	-	-	-2	-3.0	0.6
5	+4	0	+4	-	0	+1	+1.8	0.9
6	-2	-2	-	-	-6	-2	-3.0	1.0
average of column	+1.6	-0.2	+0.8	-0.3	-1.6	-0.8		
standard error of mean, = std dev/ \sqrt{n}	1.2	0.8	1.7	2.6	1.2	0.5		

Note: For higher values of δ , the percent deviations are known to greater precision and are so shown.

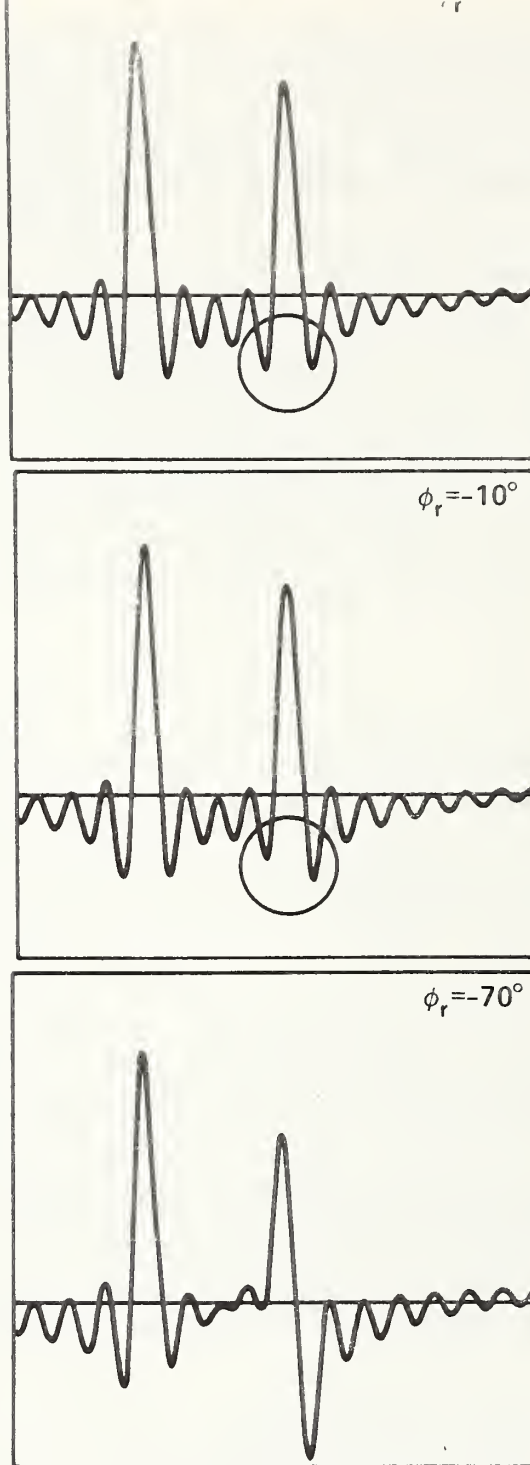


Figure 10. Examples of Predicted Correlograms
 a) $\phi_r = 0^\circ$. b) $\phi_r = -10^\circ$. c) $\phi_r = -70^\circ$

Note that the frequency dependence of C_T has been totally ignored in the above analysis. Effects of frequency dependence can be studied by further analytic modeling, that is, by assuming a frequency dependence and generating the corresponding correlograms; and also by use of cross spectral density functions, the Fourier transform of the cross-correlation functions (see especially Refs. 20 and 23).

5.8. Corrections for Wind Gradients

Effects of wind and temperature gradients were studied in some detail. The principal effects are derived in Section 7, using the geometrical (ray) acoustics limit. These effects are changes in path length difference, changes in glancing angle (thereby changing the value of β to be deduced from the measured C), and focusing effects which change the relative peak heights in the correlogram. Corrections for these effects were applied to the data in the hope of reducing the scatter.

Average wind speed was derived from the position of the first correlogram peak. This peak is located at time delay $\tau = \Delta$, where $\Delta = (R_1 - R_s)/c'$. Here R_1 is the distance traveled by the direct ray, R_s the distance to the near-field microphone, and c' the effective sound speed $c' = c + w \cos \theta$ (c is the speed of sound in still air, w is the wind speed, and θ is the angle between the wind direction and the direction of propagation of the sound). Because the wind speed varies with z , the height above the ground, a specific dependence had to be assumed, first to reduce all data to a standard height of 1.2 m, and then for use in determining the wind gradient. A one-fourth power law, $w \propto z^{1/4}$, was assumed (see Section 7.8). The wind direction was taken to be from the south, based on observation at the time of the experiment and on EPA wind data from the date in question. This assumption was consistent with the first peak data. With θ defined, w was deduced from the positions of the first peaks to be 1.4 m/s; the standard deviation of these measurements, however, was 1 m/s. The large scatter in wind data is attributed to actual variability of the wind, poor knowledge of the wind direction, incorrect assumptions about the z -dependence, insufficient precision in the measurement of microphone positions, and incomplete calibration of the analog time delay unit in the data reduction circuitry.

Each wind measurement is itself an average over several minutes of wind history, since the datum is inferred from a correlogram computed from several minutes of recorded sound signal. Since the six far-field microphones provided data simultaneously, the complete set of 30 wind measurements were grouped, each group consisting of six simultaneous measurements. Scatter within these groups was not significantly lower than the scatter between groups, as determined by an F-test (Ref. [18]). In other words, the variability between simultaneous measurements (same source position, different microphones) was comparable to the variability between successive measurements (different source positions). Thus the actual variability of the wind cannot account for the measurement uncertainty. Positional errors of 2-3 cm in microphone placement could account for these uncertainties, as could substantial departures from a $z^{1/4}$ dependence on height. (Analysis of the noise data taken at ground level might well resolve some of these questions; this additional investigation is beyond the scope of the present study.)

In fact a wind speed of 0.9 m/s was actually used in applying the corrections. This was based on the observation that a gross overestimate of wind corrections would result in "corrected" data scattered as much as the data without any corrections; however a large underestimate should still show improvement (reduction) in the data scatter. Results of applying these wind gradient corrections are also presented in Table 4. The notation β^w is used in Table 4 to represent wind-corrected measurements. Although individual measurements of β were affected, the averaged specific admittance ratio is still $\beta = .007$, with a standard deviation of .004. No improvement resulted in the plot (not shown) of C_r vs. $1/\sin \alpha$ either.

5.9. Corrections for Temperature Gradients

The ray acoustics corrections for a simple temperature gradient were also applied. Average air temperature was deduced from the measured sound speed; pad temperatures were known from on-site measurements. Differences between air and pad temperatures ranged from 2°C to 8°C during the testing period, the pad being always warmer. In order to underestimate rather than overestimate, a change in temperature of 1.5°C was postulated, together with a $z^{1/4}$ dependence on height. The effect of even this small a temperature gradient on the wind-corrected data would be to lower the averaged specific admittance ratio to $\beta = .006$, leaving the standard deviation unchanged at .004. However, the propagation time difference δ would then change by amounts of 0.05 ns or so, easily large enough to be ruled out by the measured values of δ . Thus the measured propagation time differences indicate that there was no significant temperature gradient during this test. In other words, although a measured difference existed between pad temperature and air temperature, the gradients implied by these differences and extending from ground to microphone height were ruled out, based on ray acoustics analysis. However, it is recognized that large gradients may exist in a small boundary layer at the pad surface. In this case the ray acoustics analysis would require more detailed examination.

Analysis of the noise data taken at ground level, and autocorrelations of the far-field data, might provide yet additional information, especially regarding wind gradients. Cross-correlation of filtered signals might eliminate much of the directivity effects.

6. DIRECT ACCELEROMETER MEASUREMENT

6.1. Description of Technique

This technique measures the response of the asphalt itself to an applied sound field. A pure tone source is directed at a point on the surface, the sound pressure at the surface is picked up by a microphone, and the normal velocity of the surface is sensed by an accelerometer rigidly mounted directly on the surface. The specific acoustic admittance, which is by definition the normal velocity of the air at the surface divided by the sound pressure, is computed directly. Both magnitude and phase can be readily measured, although calibration of the phase response of the microphone and accelerometer (as well as the amplitude sensitivity) is required.

However, the accelerometer at best measures only the motion of the surface material. Motion of air molecules permitted by surface roughness or porosity cannot be detected. Thus this measured ratio of asphalt velocity to acoustic pressure must be considered as a lower bound of the specific admittance (upper bound of the specific impedance) of the surface as an acoustic element.

Such a lower bound is useful, however, in that it indicates a limit to the sensitivity which may be required of other impedance measurement techniques. Equivalently, the lower bound obtained from this measurement, together with the sensitivity-limited values of β obtained by other techniques, may be considered to bracket the true specific acoustic admittance ratio of the surface.

6.2. Advantages and Limitations

Since the measurements are conducted using steady pure tones, both microphone and accelerometer output can be filtered with (matched) narrow-band filters. Thus the signal-to-noise ratio can be made so high as to be of no further concern. Moreover, since only the sound field in the immediate vicinity of the accelerometer is of interest, wind turbulence, source directivity, non-planar wavefronts, and other perturbations of the propagation path are all irrelevant.

Several potential difficulties with this procedure were resolved during the experiment. The effect of the accelerometer cable capacitance on accelerometer sensitivity may be substantial, but can be accounted for by proper calibration. The accelerometer mass may affect the surface response, and the physical size of the accelerometer may shield the asphalt from the incident signal sufficiently to affect the measurement. Direct acoustic excitation of the accelerometer may also occur. By repeating the experiment with two accelerometers of quite different size and mass, and obtaining comparable results (within 10-20%), dominating effects of size and mass were felt to be ruled out. Further, any such shielding or mass loading would generally be expected to lower the measured value of β ; thus the interpretation of this measurement as a lower bound to the true value of β is unchanged. Direct excitation of the accelerometer was ruled out by measuring much higher impedances on another surface. Clearly, mounting of the accelerometers must be done with care, to effect a rigid bond with the surface.

6.3. Experiment

The direct accelerometer measurement was performed on the asphalt in a parking area at the National Bureau of Standards, Gaithersburg, MD. (This experiment was added to the study well after the other techniques had been tested at Sandusky.) The experimental setup is depicted in Fig. 11, and the equipment configuration is presented in Fig. 12. A siren horn was used as the sound source because of its high efficiency. (Uneven frequency response and harmonic distortion are irrelevant, since both microphone and accelerometer signals are filtered. Also, the frequency is swept slowly, so that the variation in sound pressure, resulting from changes in speaker efficiency with frequency, occurs slowly compared to amplifier, filter, and detector response times.) With the siren, sound pressure levels of 100-110 dB at the surface were easily achieved. These produced acceleration levels greater than 60 dB re 10^{-6} g which, when filtered with the 5-Hz bandwidth tracking filter, were at least 30 dB above ambient vibration levels and instrument noise at all frequencies from 300 Hz to 2000 Hz.

A frequency scan, with automatic plotting of the specific impedance ratio, was performed under several conditions. Two different accelerometers were used: a Bruel and Kjaer #4332, 14 mm in diameter with a mass of 30 g, and a Bolt Beranek and Newman #501, 7 mm in diameter with a mass of 2 g. Source height was also varied from 15 cm to 1 m. The larger accelerometer was screwed onto a threaded mounting plate that had been epoxied onto the asphalt; the smaller accelerometer was bonded to the smooth surface made by applying a few drops of epoxy resin on the top of the asphalt.

6.4. Results

The output from any particular run shows rapid fluctuations with frequency, anywhere from $\pm 10\%$ to factors of 2 in the magnitude of the specific impedance, and fluctuations of about $\pm 10^\circ$ in the phase (Figure 13). The details of these fluctuations differ from one configuration to another (accelerometer, mounting, source height). However, visual inspection of these fluctuating curves allows one to estimate a smoothed response, i.e., a curve following roughly the mean of the excursions. These smoothed data are consistent, from one configuration to another, to within about 20%, over a frequency range from 500 Hz to 2000 Hz.

These smoothed data indicate magnitudes of the specific acoustic admittance ratio β of about .00035 from 500 Hz to 1000 Hz, and gradually falling to about .00020 by 2000 Hz. The phase of β as measured (raw data) decreases gradually from about 0° at 500 Hz to perhaps -40° by 2000 Hz.

The phase lag of the microphone cannot be neglected. Manufacturer's specifications indicate a lag in response rising from 0° at 500 Hz, to about 10° at 1000 Hz and 20° at 2000 Hz. The accelerometer introduces no such phase shift in this frequency range; this has been confirmed by calibration relative to a known reference accelerometer. As a result, the phase in β , after correction for the microphone, is -60° at 2000 Hz rather than the -40° indicated by the raw data.

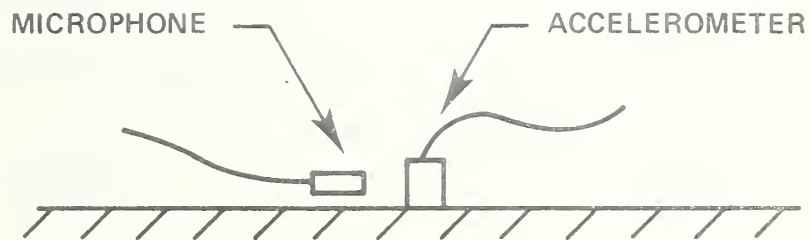
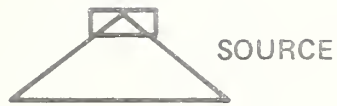


Figure 11. Sketch of Direct Accelerometer Measurement

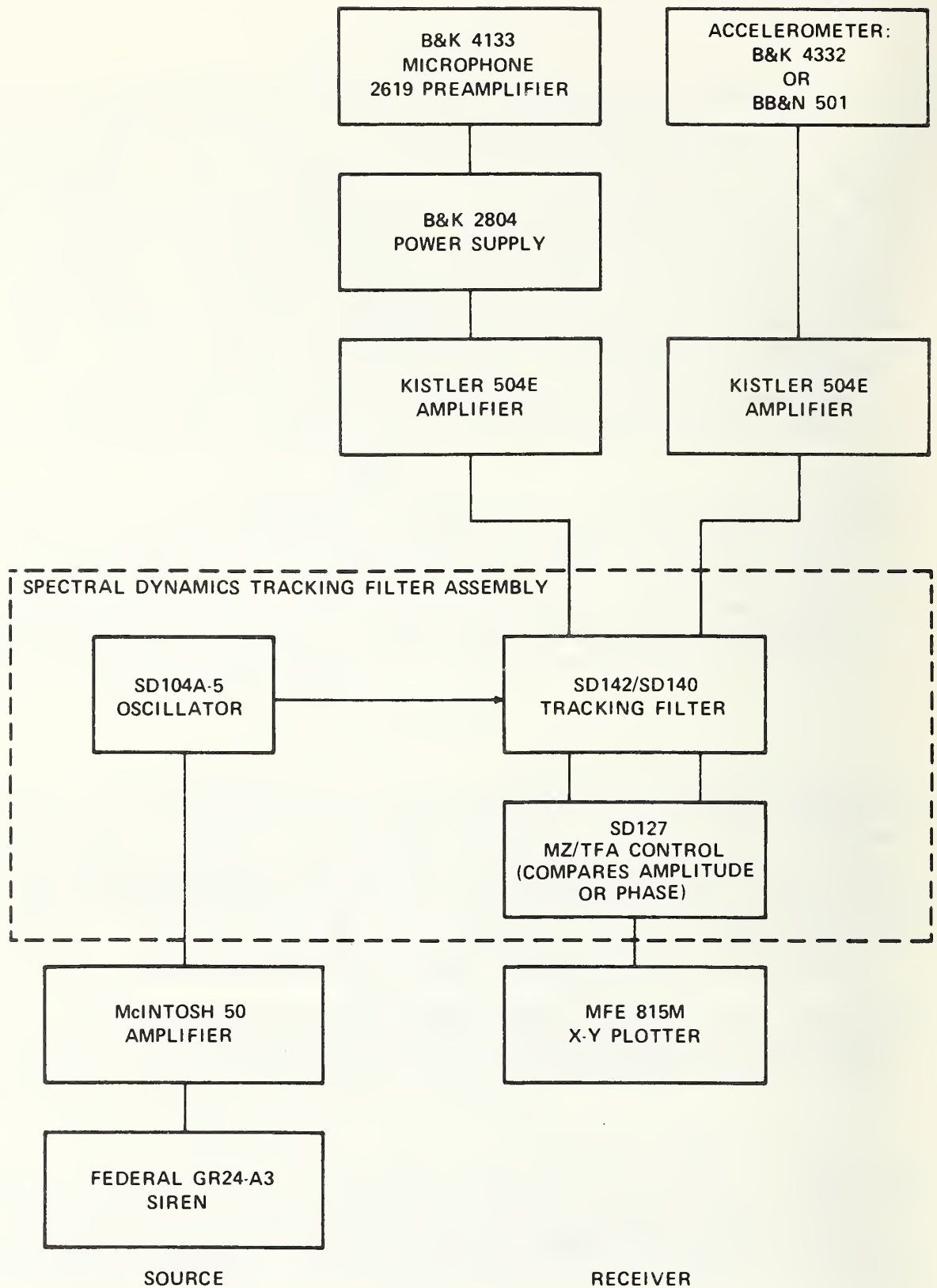


Figure 12. Block Diagram for Direct Accelerometer Measurement

Commercial instruments are identified in order to adequately specify the experimental procedure. In no case does such identification imply recommendation or endorsement by the National Bureau of Standards, nor does it imply that the equipment identified is necessarily the best available for the purpose.

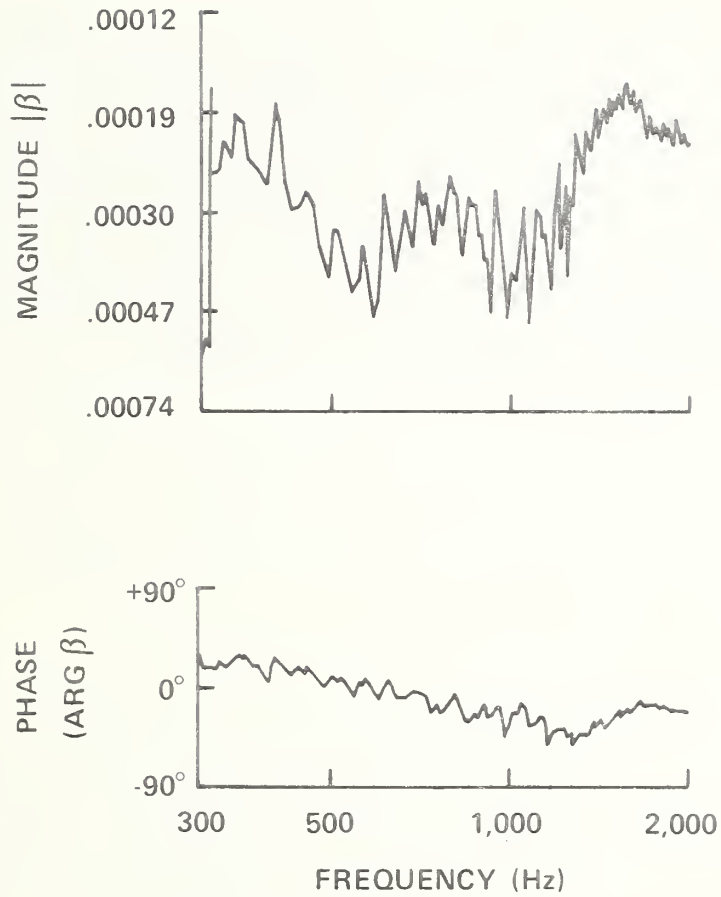


Figure 13. Output from Direct Accelerometer Measurement

Cause of the rapid fluctuations with frequency is not known. One possible cause is resonance effects within the asphalt itself (e.g., reflection from the bottom of the asphalt layer). Variation in the details of the fluctuations may well be due to changes in asphalt temperature over the period of testing. Other possible causes have been discussed, including various artifacts of the instrumentation system.

6.5. Validation

As a check on the sensitivity of this technique, the measurement was also performed on the 50 cm thick painted concrete floor of the NBS reverberation room. The smoothed data from these runs indicate specific admittance ratios as low as .00003, a factor of ten below those measured for asphalt. Moreover, these values are consistent with the value of ρc for the concrete, i.e., they represent the specific admittance due to longitudinal waves within the concrete. Variations of the smoothed data, from one configuration to another, are greater at these low measured values of β . The rapid fluctuations with frequency are also considerably greater for the concrete. If these fluctuations in fact arise from resonances within the slab itself, their increased size may result from there being less damping in concrete than in asphalt.

7. EFFECTS OF WIND AND TEMPERATURE GRADIENTS

7.1. Description of Effects

The effects of both wind and temperature on sound propagation are manifested by changes in the speed of propagation of the sound. Thus a uniform wind will increase the effective sound speed (shorten the propagation time) of a signal traveling with the wind, and decrease the speed of a signal traveling against the wind. Similarly, a higher temperature increases the local speed of sound in all directions.

In practice, wind and temperature are rarely uniform. Generally they vary with height above the ground. Wind, in particular, is constrained (by the viscosity of the air) to be zero just at the surface, and increases with height. As a result of these gradients in the wind speed and temperature, sound is refracted as it propagates. Ray paths are no longer straight lines, and propagation times are affected as well.

There are three principal effects of these gradients on measurements using the glancing-angle geometry (see e.g., Fig. 1). These are changes in the propagation time difference between direct and reflected rays; changes in the angle of incidence of the reflected ray [which therefore changes the reflection coefficient actually observed - Eq. (1-2)]; and focusing or defocusing of the reflected ray (i.e., differences in the refraction of "neighboring" rays resulting in increased or decreased intensity at the microphone). Two important "non-effects" ought to be noted: there is no significant focusing of the direct ray, and there is no change in the propagation time difference in the presence of uniform wind (zero gradient).

7.2. "Non-effect" of Uniform Wind

Although this last conclusion can be drawn from suitable limiting cases of the wind gradient corrections, a separate derivation is of interest. Care must be exercised because the propagation time difference is already a small quantity relative to the total propagation time; hence neglect of quantities small relative to the total time may not be justified. Thus, for example, having first shown that the time difference in still air is "to first order" $\delta\tau \approx 2Hh/rc$, one might suggest that in the presence of a wind component w parallel to the direction of propagation, the difference might become $\delta\tau^w = 2Hh/rc'$, where now $c' = c + w$ is the effective speed of sound. This is incorrect, since the reflected ray (at least) is not traveling parallel to the ground, but at a small angle α with respect to the horizontal. Thus the speed of this ray is only $c + w \cos \alpha$. Although the difference is slight, it applies to the entire time of propagation, and its effect on the propagation time difference cannot be neglected.

An elegant computation of this time difference can be performed in a coordinate system comoving with the wind (Figure 14). In this frame of reference the sound wave travels in still air, and its behavior is fully understood. However, the source and the microphone are moving with speed $-w$.

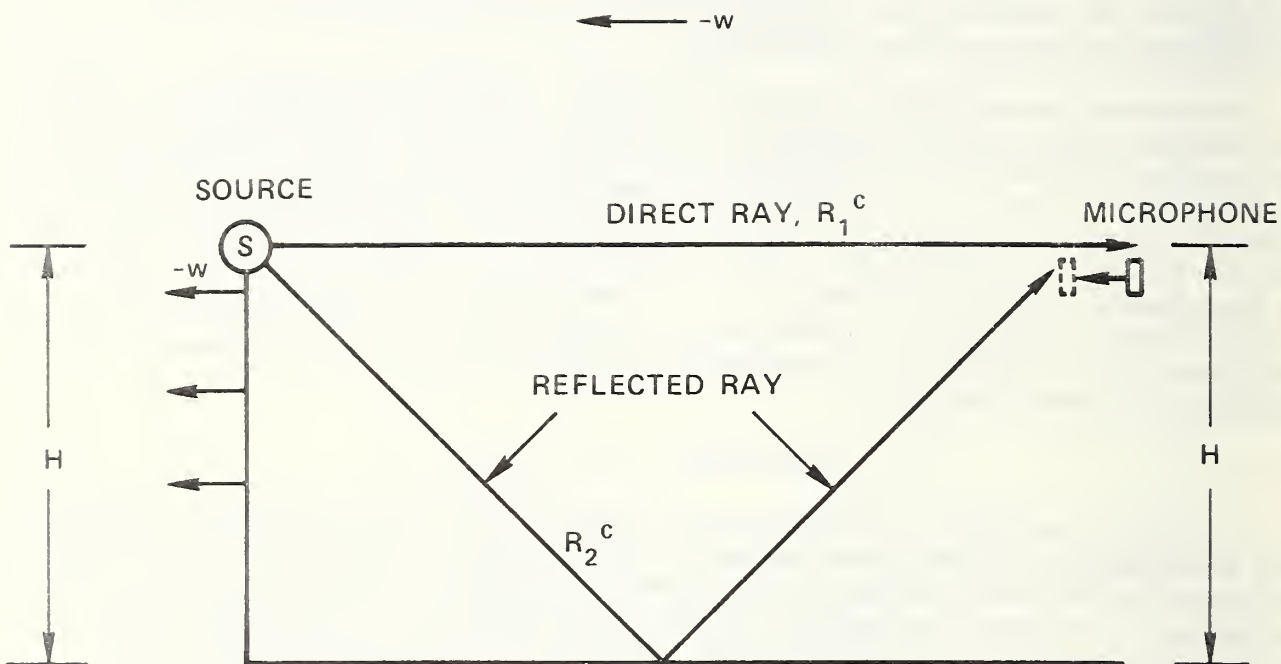


Figure 14. Ray Geometry in Comoving Coordinates

Thus in the time T_1 taken by the direct ray to travel to the microphone, the microphone has moved by an amount $-wT_1$. The distance traveled by the direct signal, in the comoving frame, is

$$R_1^c = r - wT_1 \quad (7-1a)$$

when both source and microphone are at the same height; here r is the horizontal separation of the source and microphone. In general, for source height H and microphone height h , the distance traveled in the comoving frame is

$$R_1^c = \sqrt{(r-wT_1)^2 + (H-h)^2} \quad (7-1b)$$

In either case, the transit time of the direct signal is

$$T_1 = R_1^c / c \quad (7-1c)$$

Noting that wT_1/r is of the same order as w/c , these equations can be solved to give

$$T_1 = \frac{\sqrt{r^2 + (H-h)^2}}{c} - \frac{w}{c} \frac{r}{c} + O(w^2/c^2) \quad (7-1d)$$

Similarly,

$$\begin{aligned} R_2^c &= \sqrt{(r-wT_2)^2 + (H+h)^2} \\ T_2 &= R_2^c / c \\ T_2 &= \frac{\sqrt{r^2 + (H+h)^2}}{c} - \frac{w}{c} \frac{r}{c} + O(w^2/c^2). \end{aligned} \quad (7-2)$$

Thus

$$\delta\tau^w = T_2 - T_1 = \frac{\sqrt{r^2 + (H+h)^2}}{c} - \frac{\sqrt{r^2 + (H-h)^2}}{c} + O(w^2/c^2), \quad (7-3)$$

identical to the still air case to first order in w/c .

Throughout this section terms which are second-order in wind speed (i.e., w^2/c^2) will be neglected. Source emission measurements are generally not conducted in winds above 20 km/hr, corresponding to w/c of about .017. Neglected terms will be at worst 2% of the included terms. In the present study, w/c was consistently below .005.

7.3. Fermat's Principle

Derivations of the effects of wind and temperature gradients will be based on Fermat's principle, that the path followed by a ray between two points is the one taking the shortest time (technically, an extremum)[24]. Fermat's principle is succinct and allows efficient derivation of results. The final path equations are, of course, identical to those obtained by other authors (e.g., Morse and Ingard[25], Kriebel[26]) using brute force techniques. In addition, Fermat's principle leads directly to a useful "time-of-flight" lemma, that ray path curvature may be neglected to first order in computing propagation times.

In mathematical terms, Fermat's principle states

$$\delta T = 0 , \quad (7-4)$$

where $T = \int ds/c$ is the propagation time, and δ signifies an infinitesimal variation of the ray path, keeping its end points fixed. The path itself may be parameterized by $z(x)$, where z is the height above the ground and x is the (horizontal) distance along the ground.

Wind and temperature are assumed to vary only with height, so that the sound speed c is a function of z only. For a wind component $w(z)$ parallel to the plane of propagation, $c = c_o + w(z) \cos \alpha(z)$, where c_o is the sound speed at the reflecting surface, $z = 0$. Writing $z' = dz/dx$, one gets $\cos \alpha(z) = [1 + z'^2]^{-1/2}$; also $ds = [dx^2 + dz^2]^{1/2} = dx[1 + z'^2]^{1/2}$.

For a temperature profile $\theta(z)$,

$$c(z) = c_o \sqrt{\frac{\theta(z)}{\theta(0)}} \approx c_o - \frac{1}{2} c_o \frac{\theta(0) - \theta(z)}{\theta(0)} \quad (7-5)$$

(neglecting terms in $[\theta(0) - \theta(z)]^2 / [\theta(0)]^2$) so that the effects of temperature gradients can be equally well described by using an equivalent wind profile

$$w^T(z) = - \frac{1}{2} c_o \frac{\theta(0) - \theta(z)}{\theta(0)} . \quad (7-6)$$

Then $c(z) = c_o + w(z) \cos \alpha + w^T(z)$. Only the true wind term will be examined here; the derivation of temperature effects clearly follows the same logic. It should be noted, however, that the ray acoustics limit which has been used may not be valid near the surface, since temperature in particular (but also wind speed) may change markedly within a wavelength.

7.4. Time-of-Flight Lemma

This lemma states that, in computing the propagation time of a ray to first order in w/c , it is sufficient to integrate along the straight line (zero wind)

path, rather than the curved path actually followed in the presence of wind gradients.

This lemma is based on the following reasoning. For small values of w/c , the change in ray path due to the wind is also small, i.e., first order in w/c . Since, however, the new ray path is an extremum of the time of flight T (by Fermat's principle), small deviations from the new path - for example the old zero-wind path - give rise to the same time of flight, to first order in w/c . It is important to recognize that the integrand still includes the wind terms. In other words, the wind affects the propagation time integral in two ways: it changes the integrand itself, and it changes the path of integration. This time-of-flight lemma allows one to neglect the change in the path of integration, when computing first-order effects.

Formally, let the actual ray path be written as

$$z(x) = z_0(x) + \lambda z_1(x) , \quad (7-7)$$

where z_0 is the path in the absence of wind, and $\lambda = w/c \ll 1$. (If $w < 0$, the inequalities are reversed; the proof is otherwise identical.) Then the time of flight integral may be represented as a function of the path of integration as $T(\lambda)$. Using Taylor's theorem [27],

$$T(\lambda) = T(0) + \lambda T'(0) + \frac{1}{2} \tilde{\lambda}^2 T''(\tilde{\lambda}) \quad (7-8)$$

for some $\tilde{\lambda}$ such that $0 < \tilde{\lambda} < \lambda$. Similarly,

$$T'(\lambda) = T'(0) + \tilde{\tilde{\lambda}} T''(\tilde{\tilde{\lambda}}) , \quad (7-9)$$

where also $0 < \tilde{\tilde{\lambda}} < \lambda$.

But Fermat's principle implies that $T'(\lambda) = 0$ for $\lambda = w/c$. Thus Eq. (7-9) becomes

$$T'(0) = -\tilde{\tilde{\lambda}} T''(\tilde{\tilde{\lambda}}) . \quad (7-10)$$

Inserting in Eq. (7-8),

$$T(w/c) = T(0) - (w/c) \tilde{\tilde{\lambda}} T''(\tilde{\tilde{\lambda}}) + \frac{1}{2} \tilde{\lambda}^2 T''(\tilde{\lambda}) . \quad (7-11)$$

Since both $\tilde{\lambda}$ and $\tilde{\tilde{\lambda}}$ are less than w/c , these last two terms are of second order in w/c , and can be neglected provided T'' is suitably bounded. Thus $T(w/c) = T(0)$ to first order in w/c .

7.5. Effect on Propagation Time Difference

Using this lemma, the time difference between the direct and reflected signals can be computed by integrating along the zero-wind straight line paths $z(x) = z_0 + z_0' x$, where z_0 and z_0' are constants. For the glancing-angle geometry, $z_0'^2 \ll 1$ and power series expansions in $z_0'^2$ as well as in w/c can be applied. As mentioned earlier, however, terms up to $z_0'^4$ and $z_0'^2 w/c$ must be retained in computing path length differences. Thus

$$\begin{aligned}
 T &= \int \frac{ds}{c(z)} = \int_{x_1}^{x_2} \frac{dx \sqrt{1+z'^2}}{c_0 + w(z) \cos \alpha} = \frac{1}{c_0} \int_{x_1}^{x_2} \frac{dx \sqrt{1+z'^2}}{1 + \frac{w(z)}{c_0} / \sqrt{1+z'^2}} \\
 &\approx \frac{1}{c_0} \int_{x_1}^{x_2} dx \left(1 + \frac{1}{2} z'^2 - \frac{1}{8} z'^4 - w(z)/c_0 \right) \\
 &= \frac{1}{c_0} \int_{x_1}^{x_2} dx \left(1 + \frac{1}{2} z'^2 - \frac{1}{8} z'^4 \right) - \frac{1}{c_0 z_0'} \int_{z_1}^{z_2} \frac{w(z)}{c_0} dz.
 \end{aligned} \tag{7-12}$$

Writing T^0 for the zero-wind time, and defining

$$I_w(z) = \int_0^z w(\tilde{z}) d\tilde{z}, \tag{7-13}$$

one obtains

$$T^w = T^0 - \frac{I_w(z_2) - I_w(z_1)}{c^2 z_0'}. \tag{7-14}$$

For a source height H and receiver height h , and horizontal distance r , the direct ray propagation time becomes

$$T_{\text{dir}}^w = T_{\text{dir}}^0 - \frac{1}{c_0} \frac{r}{H-h} [I_w(H) - I_w(h)] \tag{7-15a}$$

if $H \neq h$; or

$$T_{\text{dir}}^w = T_{\text{dir}}^0 - \frac{r}{c_0} \frac{w(h)}{c_0} \tag{7-15b}$$

if $H = h$, as obtained directly from the integral dx .

The reflected ray is computed as two straight line segments. Combining the propagation time for the two segments, the total reflected ray propagation time becomes

$$T_{\text{refl}}^w = T_{\text{refl}}^o - \frac{1}{c_o} \frac{r}{2(H+h)} [I_w(H) + I_w(h)]. \quad (7-16)$$

The wind-corrected path delay difference is thus

$$\delta\tau^w = T_{\text{refl}}^w - T_{\text{dir}}^w = \begin{cases} \delta\tau^o + \frac{2r}{c_o} \frac{hI_w(H) - hI_w(h)}{H^2 - h^2} & (H \neq h) \\ \delta\tau^o + \frac{r}{c_o} \left[w(h) - \frac{I_w(h)}{h} \right] & (H = h) \end{cases} \quad (7-17)$$

For the frequently postulated power law $w(z) \propto z^{1/n}$, these expressions become

$$\delta\tau^w = \begin{cases} \delta\tau^o + \frac{n}{n+1} \frac{r}{c_o} \frac{2Hh}{H^2 - h^2} \left[\frac{w(H)}{c_o} - \frac{w(h)}{c_o} \right] & (H \neq h) \\ \delta\tau^o + \frac{1}{n+1} \frac{r}{c_o} \frac{w(h)}{c_o} & (H = h) \end{cases} \quad (7-18)$$

For a uniform wind (zero gradient), $n \rightarrow \infty$ and $\delta\tau^w = \delta\tau^o$ as proved earlier.

Physically, the time delay difference arises because the reflected ray travels closer to the ground, hence through regions of lower wind speed, than the direct ray. It is not carried along as fast, and arrives later than it would were the wind uniform with height. For rays traveling against the wind ($w < 0$), the reflected ray is not slowed as much as the direct ray, and arrives sooner.

7.6. Effect on Angle of Incidence

To obtain corrections for the angle of incidence and intensity of the reflected ray, it becomes necessary to solve for the curved ray paths in the presence of wind gradients (see Figure 15). In this case, terms in z'^4 and $z'^2 w/c$ can be neglected, as these will modify the already small corrections by at worst 10% for the glancing-angle geometries with $\alpha < 20^\circ$, and more typically by only a few percent.

Fermat's principle again provides a direct derivation. Using the expression derived above:

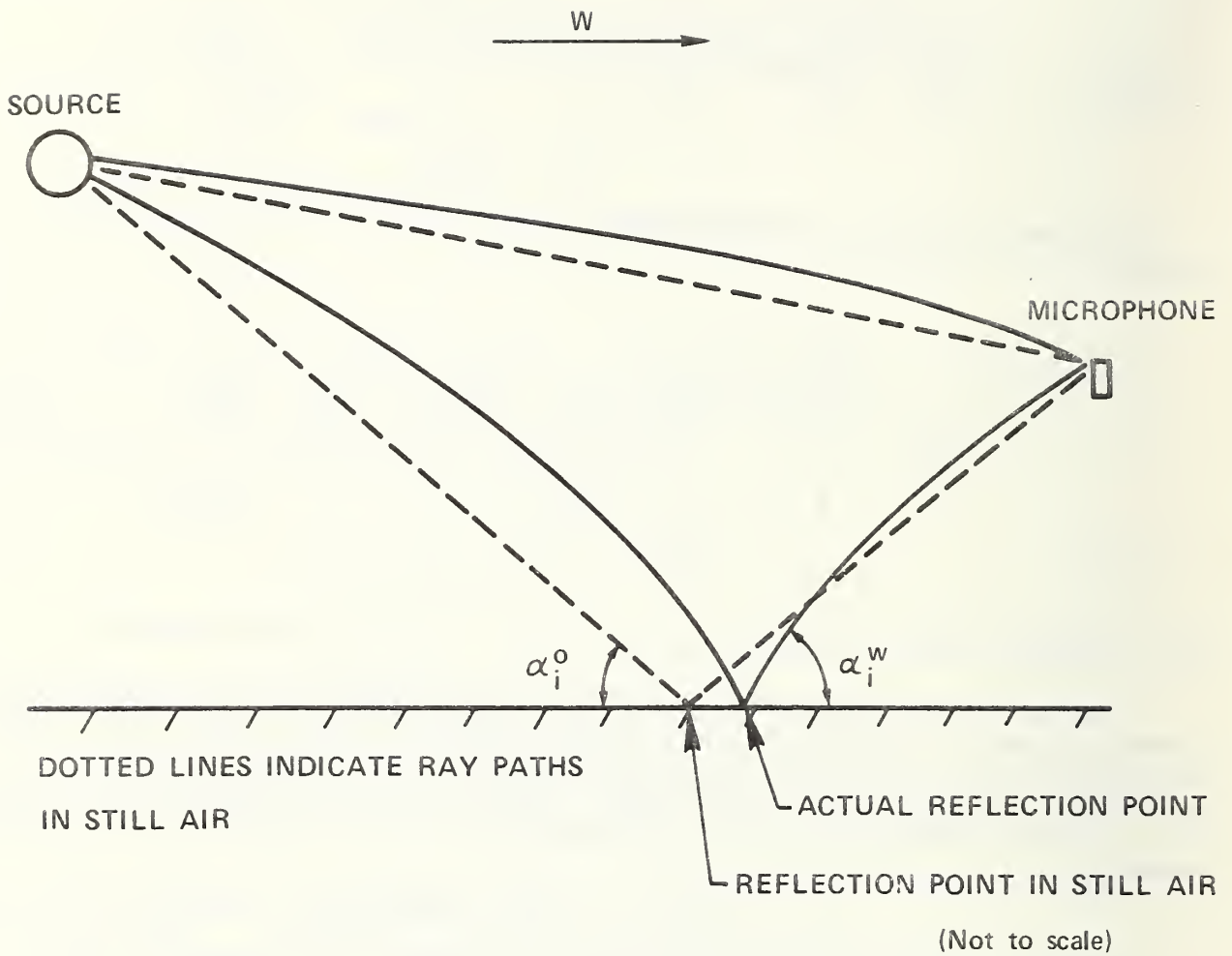


Figure 15. Ray Paths in the Presence of a Wind Gradient

$$T \approx \frac{1}{c_0} \int_{x_1}^{x_2} dx \left(1 + \frac{1}{2} z'^2 - w(z)/c_0 \right) \quad (7-19)$$

Variation of the integral ($\delta T = 0$) gives rise to

$$\left(\frac{\partial}{\partial z} - \frac{d}{dx} \frac{\partial}{\partial z'} \right) \left(1 + \frac{1}{2} z'^2 - w(z)/c_0 \right) = 0 \quad (7-20)$$

for the ray path equation (see any standard text on classical mechanics; e.g., Goldstein[10]). This can be integrated to obtain

$$\frac{dz}{dx} = \sqrt{C_1 - 2w(z)/c_0} \quad (7-21)$$

where C_1 is a constant determined by the end points of the ray path. Thus, choosing $x = 0$ at the reflection point (for the reflected ray), and using the physically necessary condition $w(0) = 0$, one gets $C_1 = z_0'^2$, and

$$\frac{dz}{dx} = \sqrt{z_0'^2 - 2w(z)/c_0} \quad (7-22)$$

This can be rewritten in integral form as

$$x = \int_0^z \frac{dz}{\sqrt{z_0'^2 - 2w(z)/c_0}} \quad (7-23)$$

For the case of $w(z) \propto z^{1/n}$ Eq. 7-23 can be integrated analytically (Appendix D). The resulting expressions, for $n > 2$, are complicated.

Instead, for situations in which $z_0'^2 \gg 2w(z)/c_0$, the integrand may be expanded as a power series in $2w(z)/c_0 z_0'^2$. For the truck measurement geometry (as used in this study), this approach is valid for wind speeds up to at least 2 m/s (5mph). Then

$$x \approx \int_0^z \frac{dz}{z_0'} \left(1 + \frac{1}{z_0'^2} \frac{w(z)}{c_0} \right) = \frac{z}{z_0'} + \frac{1}{c_0 z_0'^3} I_w(z) \quad (7-24)$$

$$z(x) \approx z'_0 x - \frac{1}{c_0 z_0'^2} I_w(z(x)). \quad (7-25)$$

Since I_w/c_0 is already of first order in w/c , its argument $z(x)$ need only be carried to "zereth" order, i.e., $z(x) = z'_0 x$.

z'_0 has been defined as the slope of the actual curved ray path at the point of reflection. Equivalently, $z'_0 = \tan \alpha_1^w$, where α_1^w is the angle of incidence (measured from the horizontal) in the presence of a wind profile. In the absence of wind, the angle of incidence α_1^0 is given by $\tan \alpha_1^0 = (H+h)/r$. Further simplification of Eq. 7-25 may thus be obtained, since $z'_0 = \tan \alpha_1^0 + O(w/c)$, and $\tan \alpha_1^0 \approx \alpha_1^0 - (\alpha_1^0)^3/3 = (H+h)/r + \text{terms smaller by } (H+h)^2/r^2$. (α_1^0 must be expressed in radians for the power series expansions in this section.) To first order, then

$$z(x) \approx z'_0 x - \frac{1}{c_0 (\alpha_1^0)^2} I_w(z(x)). \quad (7-26)$$

In order to obtain the wind-corrected angle of incidence ($\arctan z'_0$), it is necessary to know the point of incidence, which also may shift in the presence of wind (see Fig. 15). Letting x_1 represent the horizontal distance between the source and the point of incidence, and x_2 the corresponding distance between the point of incidence and the microphone, Eq. (7-26) becomes

$$H = z'_0 x_1 - \frac{1}{c_0 (\alpha_1^0)^2} I_w(H) \quad (7-27)$$

$$h = z'_0 x_2 - \frac{1}{c_0 (\alpha_1^0)^2} I_w(h).$$

Since $x_1 + x_2 = r$ and $\alpha_1^0 \approx (H+h)/r$, these equations reduce to

$$z'_0 = \frac{H+h}{r} + \frac{1}{c_0} \frac{r}{H+h} \frac{I_w(H)+I_w(h)}{H+h} \quad (7-28)$$

or

$$\tan \alpha_1^w = \tan \alpha_1^0 \left\{ 1 + \frac{1}{c_0} \left(\frac{r}{H+h} \right)^2 \frac{I_w(H)+I_w(h)}{H+h} \right\} \quad (7-29)$$

For the case $w(z) \propto z^{1/n}$, this becomes

$$\tan \alpha_i^w = \tan \alpha_i^o \left\{ 1 + \frac{n}{n+1} \frac{1}{c_o} \left(\frac{r}{H+h} \right)^2 \frac{Hw(H)+hw(h)}{H+h} \right\}. \quad (7-30)$$

Note in particular that, given that $n > 2$, the precise value of n is not terribly important in determining an approximate correction. Since

$\beta = \frac{1 - C_r}{1 + C_r} \sin \alpha_i$ and $\sin \alpha_i \approx \tan \alpha_i$, the multiplier in braces in Eq. (7-30) can be applied directly to the β obtained from impedance measurements at glancing angles, to account for the change in angle of incidence due to wind gradients.

7.7 Focusing Effect

An additional correction is required, however, due to focusing of the reflected rays in the vertical plane. Figure 16 presents a diagram. Two "neighboring" rays are emitted, one (solid line) with slope z_e' , the other (dashed line) with slope $z_e' + \delta z_e'$, from the source at height H . The first ray impinges on the surface at a point x_1 away (horizontal distance), and at an angle of incidence α_i . This ray is reflected, and arrives at the microphone at height h , a (horizontal) distance r from the source, or equivalently $r - x_1$ from the reflection point. The second ray impinges on the surface at a somewhat different point, $x_1 + \delta x_1$ away, and at an angle of incidence $\alpha_i + \delta \alpha_i$. This ray reaches the height of the microphone at a point $r + \delta r$ from the source. At the microphone, however, its height is $z(r)$, different from h by an amount δz_r . The distance between the two rays is $\delta z_r \cos \alpha_r$, where α_r is the angle of the ray path with the horizontal. The energy contained in the emitted ray bundle $\delta z_e'$ is also contained in the rays spanned by $\delta z_r \cos \alpha_r$. The intensity is thus proportional to $(\delta z_r \cos \alpha_r)^{-1}$, and the pressure amplitude is proportional to the square root of this. Thus, defining M_w as the ratio of the amplitude in the presence of wind to the amplitude in still air,

$$M_w = \sqrt{\frac{\delta z_r^o \cos \alpha_r^o}{\delta z_r^w \cos \alpha_r^w}} \quad (7-31)$$

provided the same emission angle $\delta z_e'$ is used.

The derivation is straightforward but tedious. The first ray path is described by

$$z_1(x) = z_o'x - \frac{1}{c_o \alpha_i^2} I_w(\alpha_i x) \quad (7-32)$$

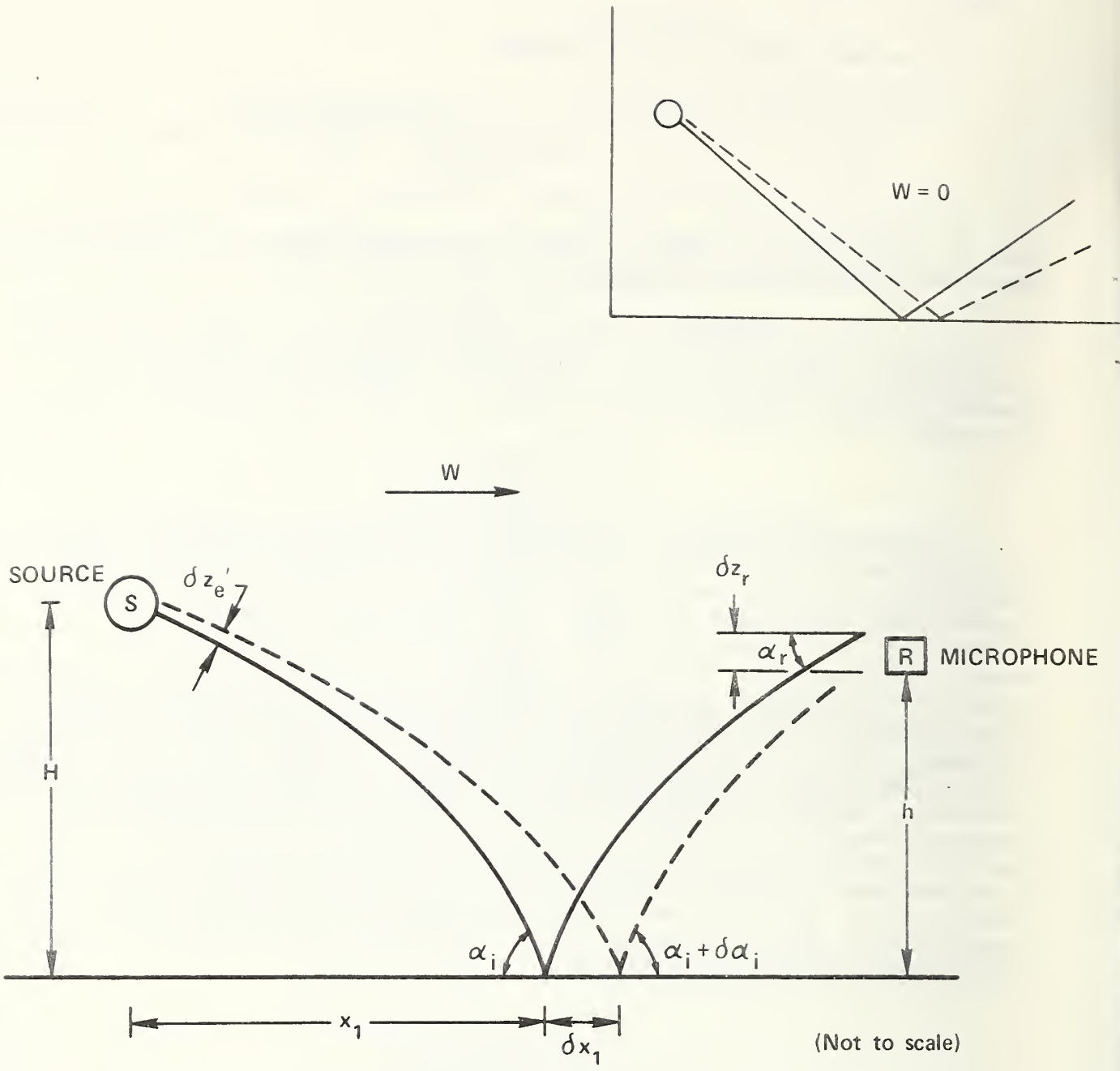


Figure 16. Ray Diagram for Focusing Effect

where $x = 0$ is at the reflection point. On the incident side, the source is at $x = x_1$, $z = H$; the emission angle is $z_e' = \frac{dz}{dx} \Big|_{x=x_1}$. On the reflected side, the microphone is at $x = r - x_1$, $z = h$; $\alpha_r = \arctan \frac{dz}{dx} \Big|_{x=r-x_1}$. The second ray path is described by

$$z_2(x) = (z_o' + \delta z_o')x - \frac{1}{c_o(\alpha_i + \delta\alpha_i)^2} I_w((\alpha_i + \delta\alpha_i)x). \quad (7-33)$$

Again $x = 0$ is taken at the reflection point. As a result, the source is at $x = x_1 + \delta x_1$, $z = H$; $z_e' + \delta z_e' = \frac{dz}{dx} \Big|_{x=x_1+\delta x_1}$. The microphone is at $x = r - (x_1 + \delta x_1)$, at which point the ray is at height $z(x) = h + \delta z_r$. It is only necessary to evaluate δz_r as a function of $\delta z_e'$. Terms which are second-order (or higher) in the infinitesimal quantities are always discarded.

Thus the condition $H = z_1(x_1) = z_2(x_1 + \delta x_1)$ leads to

$$z_o' \delta x_1 + (x_1 - \alpha_i^2 x_1 + \frac{2}{c_o \alpha_i^3} I_w(H)) \delta \alpha_i = 0 \quad (7-34)$$

(using also $z_o' = \tan \alpha_1 \approx \alpha_1 + \alpha_1^3/3$). The definitions

$$z_e' = \frac{dz_1}{dx} \Big|_{x=x_1} \text{ and } z_e' + \delta z_e' = \frac{dz_2}{dx} \Big|_{x=x+\delta x_1} \text{ lead to}$$

$$\delta z_e' = \left(1 - \alpha_i^2 + w(H)/c_o \alpha_i^2 \right) \delta \alpha_i. \quad (7-35)$$

The condition $h = z_1(r - x_1)$ and the definition $h + \delta z_r = z_2(r - x_1 - \delta x_1)$ lead to

$$\delta z_r = -z_o' \delta x_1 + (r - x_1) \delta z_o' + \frac{2I_w(h)}{c_o \alpha_i^3} \delta \alpha_i - \frac{w(h)}{c_o \alpha_i^2} \delta z_r. \quad (7-36)$$

Combining,

$$\delta z_r = r \delta z_e' \left\{ 1 + \frac{2(I_w(H) + I_w(h))}{c_o \alpha_i^3 r} - \frac{w(H) + w(h)}{c_o \alpha_i^2} \right\}, \quad (7-37)$$

where terms of order $\alpha^2 w/c$ have been neglected. The factor $\cos \alpha_i \approx 1 - \alpha_i^2/2$ [see Eq. (7-31)] leads to corrections smaller by a factor of α^2 than the remaining terms, and will be neglected for this study. Note in passing, however, that although still-air expressions for α_i may be used in the terms which are already of order w/c , wind-corrected values for α_i would have to be used in the $\alpha_i^2/2$ term, in the expansion of $\cos \alpha_i$.

It may be noted that there is also some focusing in the horizontal plane. Rays are curved horizontally as well as vertically (i.e., their direction of propagation in the xy-plane changes) as they pass through layers of differing wind speed. Neighboring rays emitted at the same vertical angle z' but at slightly different azimuthal angles (in the xy-plane) are bent by differing amounts in azimuth, arriving with greater or lesser intensity at the microphone. This effect is smaller than the vertical focusing by a factor of α^2 . Thus, it is comparable to other terms which have been neglected in this study, and it will be neglected as well.

The correction factor for the reflected signal amplitude in the presence of a wind profile is thus approximately

$$M_w = \frac{p_w}{p_o} \approx 1 - \left(\frac{r}{H+h}\right)^2 \frac{I_w(H)+I_w(h)}{c_o(H+h)} + \frac{1}{2} \left(\frac{r}{H+h}\right)^2 \frac{w(H)+w(h)}{c_o} \quad (7-38)$$

For the case $w(z) \propto z^{1/n}$,

$$M_w \approx 1 + \frac{1}{2} \frac{r^2}{(H+h)^3} \left[\left(h \frac{n-1}{n+1} H \right) \frac{w(H)}{c_o} + \left(H \frac{n-1}{n+1} h \right) \frac{w(h)}{c_o} \right] \quad (7-39)$$

The factor M_w , representing a change in the amplitude of the reflected signal, is manifested as an apparent change in the reflection coefficient. Thus, in the glancing angle measurement of reflection coefficient discussed in earlier chapters, the quantity measured was in fact $M_w C_r$ rather than just C_r . This effect of wind can be compensated for by dividing the apparent C_r by M_w to obtain the actual C_r .

A similar derivation would show that focusing of the direct ray bundle is negligible. If $H \neq h$, the direct ray path equation is similar to Eq.(7-25), but with a constant added on the right hand side. For the special case of $H = h$ ($\alpha = 0$), the constant C_1 in Eq.(7-21) becomes $C_1 = 2w(z_p)/c_o$, where z_p is the highest (or lowest) value of z occurring in the ray trajectory. From symmetry arguments, it is clear that z_p occurs at the midpoint. Using also $z_p = H + O(w/c)$, one can derive

$$z_p = H + \frac{1}{2} r^2 w'(H)/c_o \quad (7-40)$$

$$z(x) = H + \frac{1}{2} x(r-x) w'(H)/c_o \quad (7-41)$$

for the direct ray path when $H = h$. In either case, the derivation of the focusing effect would proceed similarly to the above.

7.8. Wind Profile

In applying the corrections for wind gradients to the measurements performed in this study (see e.g., Section 5), a wind profile had to be postulated. A power law profile $w(z) \propto z^{1/n}$ was assumed and the value $n = 4$ was used. The selection of $n = 4$ was based on some sparse data found in the literature (Thornthwaite, [29]). Non-turbulent flow theory predicts $n = 7$ [26]; however, as noted earlier, the wind correction factors are not very sensitive to the choice of n , for $n > 2$.

Using $n = 4$, the corrections become:

$$\delta\tau^w = \begin{cases} \delta\tau^o + \frac{4}{5} \frac{r}{c_o} \frac{2Hh}{H^2-h^2} \left[\frac{w(H)}{c_o} - \frac{w(h)}{c_o} \right] & (H \neq h) \\ \delta\tau^o + \frac{1}{5} \frac{r}{c_o} \frac{w(h)}{c_o} & (H=h) \end{cases} \quad (7-42)$$

$$\tan \alpha_i^w = \tan \alpha_i^o \left\{ 1 + \frac{4}{5} \frac{r^2}{(H+h)^3} \frac{Hw(H)+hw(h)}{c_o} \right\} \quad (7-43)$$

$$M_w = 1 + \frac{1}{2} \frac{r^2}{(H+h)^3} \left[\left(h - \frac{3}{5}H \right) \frac{w(H)}{c_o} + \left(H - \frac{3}{5}h \right) \frac{w(h)}{c_o} \right] \quad (7-44)$$

The wind speed was to be specified at a height of 1.2 m, and corrected to other values of H or h using the assumed $z^{1/4}$ power law. Since only three pairs of value for (H, h) were used in the broad-band experiment, the corrections were further simplified as follows:

$$\delta\tau^w = \delta\tau^o + K_1 \frac{r}{c_o} \frac{w}{c_o} \quad (7-45)$$

$$\tan \alpha_i^w = \tan \alpha_i^o \left\{ 1 + K_2 r^2 \frac{w}{c_o} \right\} \quad (7-46)$$

$$M_w = 1 + K_3 r^2 \frac{w}{c_o}, \quad (7-47)$$

where w is the wind speed parallel to the propagation plane, at a height of 1.2 m; and the constants K_i take on the following values:

H,h	(meters)	1.2,1.2	1.2,2.4	2.4,2.4
K_1	(s^{-1})	.20	.20	.24
K_2	(m^{-2})	.135	.068	.040
K_3	(m^{-2})	.034	.015	.010

The results of applying these corrections to the measurements obtained in this study have been discussed in earlier sections.

8. SPHERICAL WAVEFRONT CORRECTIONS

8.1. Correction Expressions

For a flat locally reacting surface with a given specific acoustic admittance ratio β , the reflection coefficient for plane waves is given by

$$C_{rp} = \frac{\sin \alpha - \beta}{\sin \alpha + \beta} \quad (8-1)$$

For the case of sound emission from a localized source, the incident waves are not plane; at best they are approximately spherical, and the reflection coefficient given by C_{rp} (above) is no longer applicable. Conversely, the specific admittance ratio β inferred from the measured reflection coefficient by using Eq. 8-1 will be in error.

The problem of computing the sound field due to a point source above a plane has been addressed by a number of authors[30-34]. In deriving analytic expressions for the sound field in the limiting case of a high impedance boundary, these authors all make the assumption (among others) that $k(H+h)^2/r \ll 1$. This condition requires that the observer be so far away that the path length difference ($R_2 - R_1$) becomes a great deal smaller than one-sixth of a wavelength. For the truck measurement geometry and typical truck noise spectra, this condition is not met.

Thomasson[34] has derived an exact solution containing a single integral. Using the notation of the present paper, Thomasson's expression for the velocity potential ψ can be manipulated into the following form:

$$\psi = \frac{e^{ikR_1}}{4\pi R_1} + C_r \frac{e^{ikR_2}}{4\pi R_2} \quad (8-2a)$$

$$C_r = C_{rp} + \frac{2\beta}{\beta + \gamma} F(a) \quad (8-2b)$$

$$F(a) = \int_0^{\infty} e^{-u} \left(1 - \frac{1}{\sqrt{1 + iau}} \right) du, \quad (8-2c)$$

where

$$\gamma = \sin \alpha$$

$$C_{rp} = \frac{(\gamma - \beta)}{(\gamma + \beta)} \quad (\text{plane wave coefficient})$$

$$a = \frac{2(1 + \beta\gamma)}{kR_2(\beta + \gamma)^2}$$

In this form $F(a)$ corresponds to the function F defined by Ingard, and a is inversely proportional to his numerical distance [30]. These expressions apply for $|\beta| < 1$ and $kR_2 \gg 1$.

For small a , $F(a) \approx ia/2$ and the plane wave approximation is very good. For very large a , $F(a) \sim 1 - \sqrt{\pi/2a} + i\sqrt{\pi/2a}$ asymptotically; this is equivalent to the expressions derived by Wenzel [31] and others. For the truck noise measurement geometry, a ranges roughly from .01 to 10. The linear (small a) approximation suffices for the lower portion of this range; neither limit is very good in the upper portion.

$F(a)$ can be written exactly as

$$F(a) = 1 - (1-i)\sqrt{\frac{\pi}{2a}} w\left(\frac{1+i}{\sqrt{2a}}\right), \quad (8-3)$$

where w here is a function (related to the error function) which is tabulated in Abramowitz and Stegun, p. 325 [35]. $F(a)$ for real values of a is presented as a graph in Fig. 17.

Note that the reflection coefficient C_r given in Eq. (8-2b) does not become zero at some small angle of incidence, as it would in the plane-wave case.

8.2. Application to Impedance Measurement

In this study β has been computed from measured values of C_r using the plane-wave expression [Eq. (1-2)]. Thus, corrections due to the spherical wavefront are required. Using $F(a) \ll 1$, Eq. (8-2b) can be solved for β to give

$$\begin{aligned} \beta &\approx \beta_p (1 + 2F(a)/(1+C_r)) \\ &\approx \beta_p (1 + F(a)), \quad \text{if } C_r \approx 1. \end{aligned} \quad (8-4)$$

Here β_p is the value obtained using the plane-wave approximation. Since $\beta \ll \gamma \ll 1$, little error is introduced by using β_p (or even any nominal value of β) in computing a .

For the pure-tone traverse measurement this correction has been included in the tabulated results (Table 2). Values of a are .37, .27, and .22 at 1000 Hz, 1600 Hz, and 2000 Hz respectively, and the resulting corrections are less than 15%.

The broad-band measurement is not so easy to correct, since a and therefore $F(a)$ depend strongly on frequency, whereas the data are frequency averaged. Approximate values of $F(a)$ averaged over frequency were estimated for several pertinent values of $a' = a/f$ ranging from 75 to 450:

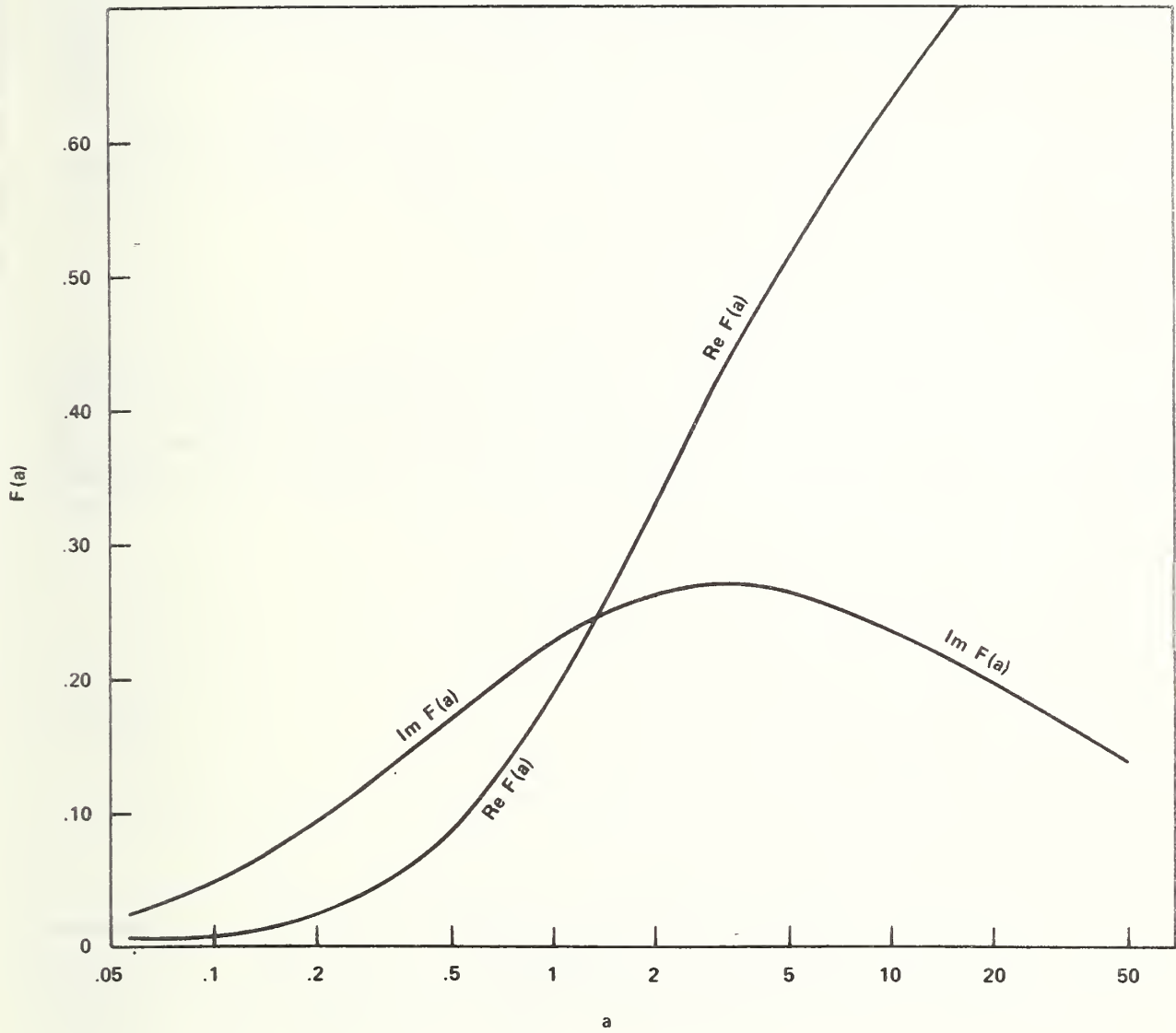


Figure 17. Graph of Function $F(a)$, for Real a (Eq. 8-2c)

a'	averaged $F(a)$
75	.01 + .041
150	.03 + .081
300	.06 + .121
450	.10 + .151

Even the worst case ($a' = 450$) resulted in corrections to the deduced value of β of only 10%. This is well below several other sources of error at the present time, and has not been included in the data reduction of Section 5.

9. EFFECT OF SURFACE IMPEDANCE ON SOURCE EMISSION MEASUREMENTS

9.1. Assumptions

The asphalt impedance measurements conducted for this study yielded specific admittance ratio values β of less than .01 for the sealed asphalt, and .02 - .06 for the unsealed, at the EPA Sandusky test site. It is of interest, then, to address the question of how serious is the uncertainty of an enforcement measurement, as a result of the uncertainty in surface impedance, given that the test site surface is a sealed asphalt surface. Further, to what extent could the measurement uncertainty be reduced, were the value of surface impedance at a given test site known more precisely.

Several assumptions will be made for this analysis. First, the surface is assumed to be locally reacting, so that the reflection coefficient is given by

$$C_r = (\gamma_i - \beta) / (\gamma_i + \beta) \quad (9-1)$$

where $\gamma_i = \sin \alpha_i$, and α_i is the angle of incidence (measured from the horizontal) of the reflected ray. Second, the truck passby measurement geometry will be assumed, so that $\gamma_i \ll 1$ (and also for the direct ray: $\gamma_d = \sin \alpha_d \ll 1$). This assumption will continue to hold for other products tested in a similar configuration. However, α_i will be assumed large enough - and β small enough - that

$$2\beta / \gamma_i \ll 1 \quad (9-2)$$

so that

$$C_r \approx 1 - 2\beta / \gamma_i \quad (9-3)$$

For specific admittance ratios of .01 and truck geometries ($\gamma_i > 0.1$) this assumption is valid. For sources closer to the ground - truck tires, motorcycles, lawnmowers - this assumption is borderline for $\beta = .01$, and becomes invalid if β is any larger. (Additional effects of wind and temperature gradients and of spherical wavefront corrections will not be considered in this Section.)

9.2. Real Admittance

For a point source, the measured signal results from the superposition of the direct and reflected signals. The reflected signal is attenuated and shifted in phase relative to the direct signal, both because of differences in the path length, and because of the effect of the surface as described by the reflection coefficient.

The mean-squared pressure for a pure tone is thus

$$p^2 = A_d^2 + A_r^2 + 2A_d A_r \cos \phi, \quad (9-4)$$

where A_d is the amplitude of the direct signal, A_r of the reflected signal, and ϕ is the total phase difference between them. In general,

$$A_r = |C_r| \frac{R_1}{R_2} A_d \quad (9-5)$$

(the attenuation on reflection multiplied by a spherical divergence factor), and

$$\phi = \phi_o + \phi_r, \quad (9-6)$$

where $\phi_o = 2\pi(R_2 - R_1)/\lambda$ is the phase change due to the path length difference, and ϕ_r is that due to reflection.

For real values of β , using the approximation $2\beta/\gamma \ll 1$, $\phi_r = 0$ and

$$A_r \approx (1 - 2\beta/\gamma_r + \frac{1}{2}\gamma_d^2 - \frac{1}{2}\gamma_r^2) A_d \quad (9-7)$$

so that

$$p^2(\beta) \approx A_d^2 \left[2(1 + \cos \phi_o) \left(1 - 2\beta/\gamma_r + \frac{1}{2}\gamma_d^2 - \frac{1}{2}\gamma_r^2 \right) \right] \quad (9-8)$$

When $\cos \phi_o = -1$, there is cancellation between direct and reflected rays, and terms in $(2\beta/\gamma)^2$ become important; these terms will be neglected in general. (The cancellation is incomplete in the presence of even a small amount of turbulence - see, e.g., Ref. 11.) The error, in decibels, resulting from β not being zero ($\beta = 0$ is the idealized measurement) is then roughly

$$e_\beta = 10 \log \frac{p^2(\beta)}{p^2(0)} \approx -9 \beta/\gamma_r \quad (9-9)$$

This is independent of ϕ_o (except when $\cos \phi_o = -1$), so that the only dependence on frequency is through β . To the degree that β is independent of frequency, the error in measuring a broad-band source is also given by Eq. 9-9.

For $\beta = .01$ and $\gamma_r = .1$ (the smallest angle generally encountered in truck passby testing) $e_\beta \approx -9$ dB, i.e., the measured level is about 1 dB less than that which would be achieved over an infinitely hard reflecting surface. (For the unsealed surface with $\beta = .02 - .06$ the approximation $2\beta/\gamma \ll 1$ is no longer valid. It is conjectured from physical grounds that the largest frequency-independent error possible is 3 dB.)

A value of .01 is believed to be an upper bound of β for the sealed asphalt surface of the Sandusky site. A better measurement, using the experience gained in this study, could indicate actual surface values of β considerably smaller. Uncertainties in measured values of noise emission due to uncertainties in the value of β would be reduced proportionately. Similarly, demonstration that the values of β at several sites were very close together would limit the noise emission measurement variability attributable to differences in site surface. However, it is not known what range of β 's might be found in comparing existing test sites, or even in comparing different points on the same test pad. It is not even known if $\beta < .01$ is typical for sealed asphalt in general.

If indeed β is real, measurements performed at a particular site could in principle be corrected for the effect of known impedance, using Eq. (9-9) above. In practice, however, sources (e.g., trucks) are not point sources, and often radiate noise from several areas, each having its own value of γ . Thus the correction is not known unless the relative contributions of the different sub-sources are known.

Assuming some realistic source distribution for truck noise emission (excluding tires), one conjectures that corrections of -0.9 dB (for $\beta = .01$) from source components at lower heights are averaged with corrections of perhaps -0.3 dB for higher components (particularly the exhaust). Thus even comparing source emission measurements at sites having $\beta = .01$ with measurements at sites having $\beta = 0$, systematic corrections would be well under 1 decibel. One may further conjecture that site to site variations in β are in fact smaller than this. It seems more promising to validate these conjectures on site variability rather than to attempt to develop meaningful site corrections.

For lower and smaller sources, however, such as truck tires, motorcycles, or lawnmowers, Eq. (9-9) may be useful in correcting measurements from different sites to some "standard" value of β .

9.3. Complex Admittance

The problem of β having an imaginary part is more complicated. Eq. (9-8) must then be written as

$$p^2(\beta) \approx A_d^2 \left[2(1 + \cos(\phi_o + \phi_r)) \left(1 - 2 \operatorname{Re} \beta / \gamma_r + \frac{1}{2} \gamma_d^2 - \frac{1}{2} \gamma_r^2 \right) \right], \quad (9-10)$$

where the phase shift now includes a term ϕ_r due to reflection, as well as that due to the path difference ϕ_o . Again, the error is $e_\beta = p^2(\beta) / p^2(0)$. If ϕ_o is less than about $\pi/2^0$ radians, this error can be expressed roughly as

$$e_\beta \approx -9 \left(\frac{\operatorname{Re} \beta}{\gamma_r} + \frac{\operatorname{Im} \beta}{\gamma_r} \tan \frac{\phi_o}{2} \right). \quad (9-11)$$

Even this restricted case depends on frequency, since $\phi_0 = 2\pi(R_2 - R_1) f/c$, so that the error in a broad-band measurement depends on the source spectrum. Moreover, the restriction $\phi_0 < \pi/2$ limits the validity of this expression to frequencies below 200-500 Hz, depending on the precise source-receiver geometry.

One result of a phase shift on reflection is to alter the frequencies at which cancellation between direct and reflected signals occurs. If the source has a very strong pure tone, the measured level could be altered by many decibels as a result of the phase shift on reflection. For realistic spectra, errors of a few (2-3) decibels are quite possible. Quantitative correction of such errors is not practical, since they would be highly sensitive to tone frequency and source-receiver geometry, and the slightest wind or temperature effects would alter the correction. Such pure-tone errors can be minimized by appropriately averaging measurements taken at several different microphone distances and/or heights.

At the other extreme of a broad-band source with a flat spectrum out to high frequencies, all frequencies are averaged, and the resulting error becomes $e_\beta = -9 \operatorname{Re} \beta/\gamma_1$, as the case with no phase shift (β real). For broad-band sources in general, it may be expected that errors at some frequencies will be partially offset by errors of the opposite sign at other frequencies, when reporting overall A-weighted levels.

By bounding $|\beta|$ and $\arg \beta$, and assuming some typical source spectra, realistic error bounds for use in field measurements may be obtained. It may be anticipated that these errors would lie in the range of 1-2 dB for $|\beta| = .01$. Additional measurements of β , at several sites, and information on actual source spectra, would be desirable before such an analysis is undertaken.

10. CONCLUSIONS

10.1. Evaluation of Techniques

Five techniques were used to measure the specific acoustic impedance of an asphalt surface. Two of these - impedance tube and direct accelerometer measurement - measure normal impedance and require the assumption of a model (such as the locally reacting point impedance model) to deduce reflection coefficients at the glancing angles of incidence relevant to source emission measurements. The other three - pure-tone traverse, pulse-echo, and broadband cross-correlation - measure reflection coefficients at glancing angles directly. It is after all these glancing angle reflection coefficients that must be known in order to interpret source emission measurements. The quantity β , as defined in Eq. (3-2), may be a convenient way of expressing the reflection coefficient. Only its interpretation as a specific admittance ratio, and its use to relate reflection coefficients at different angles of incidence, depend on the assumption of a locally reacting point impedance model.

Advantages and disadvantages of each method as used are summarized in Table 6. It is clear that further refinements are possible in all of the techniques. Some of these refinements have been discussed in earlier chapters.

The commercially available impedance tube proved to be awkward to use, limited in how high a value of impedance could be measured, and very inaccurate in measuring the phase of the impedance for very hard surfaces.

The accelerometer technique on the other hand was very sensitive. However, it measures only the mechanical part of the impedance, and ignores the effects of porosity and surface roughness on both magnitude and phase of the acoustic impedance. Its usefulness lies in providing an upper bound to the actual specific impedance, while the less sensitive methods provide lower bounds.

The pure-tone traverse provided a relatively precise measurement of phase shift on reflection, but was limited in the values of impedance that it could measure. The apparatus used was awkward to set up; thus only one point and one angle of incidence were measured. A hand-held meter traversing a path defined by a string would be simpler to set up, and would still provide useful phase shift information.

The pulse-echo experiment provided no useful impedance data. Ambient noise limited the accuracy with which signal amplitudes could be compared, although the addition of signal enhancement techniques could be expected to alleviate this problem. Phase shift information was entirely buried in noise; even under better circumstances, waveform distortion would be difficult to interpret in terms of phase shift. Speaker directivity, dependent on frequency, complicated this measurement even further.

The broad-band cross-correlation method proved to be the most promising technique for immediate application. It required a relatively simple setup, permitting collection of a lot of data, including data at different angles of

Table 6. Advantages and Disadvantages of Impedance Measurement Techniques as Used in This Study

Method	Advantages	Disadvantages
Impedance Tube	<ul style="list-style-type: none"> well-known tool no wind problems potential for using narrow band filtering commercially available 	<ul style="list-style-type: none"> difficult to use limit on how high an impedance can be measured inaccurate in measuring phase when impedance is high. requires model to deduce glancing angle properties
Direct Accelerometer Measurement	<ul style="list-style-type: none"> straightforward very sensitive - can measure very high values of impedance ambient noise not a problem unaffected by wind 	<ul style="list-style-type: none"> measures only mechanical part of impedance - ignores porosity requires careful mounting requires model to deduce glancing angle properties
Pure-Tone Traverse	<ul style="list-style-type: none"> precise measurement of phase shift potential for using narrow-band filtering 	<ul style="list-style-type: none"> difficult to set up limit on how high an impedance can be measured. affected by wind and turbulence needs non-directional source
Pulse-Echo	<ul style="list-style-type: none"> easy to set up 	<ul style="list-style-type: none"> very sensitive to ambient noise very sensitive to air turbulence poor measurement of phase shift needs non-directional source
Broad-Band Cross-Correlation	<ul style="list-style-type: none"> easy to collect lots of data can measure high values of impedance averages over turbulence provides information on wind ambient noise not a serious problem 	<ul style="list-style-type: none"> requires specialized data reduction equipment no immediate frequency information requires non-directional source with wide frequency response.

incidence and different points on the test site surface. It averages over air turbulence, and can provide its own information on wind, temperature, and their gradients. In the present experiment the results were limited in precision by source directivity. It is believed that directivity errors can quite easily be reduced to the point where values of the specific admittance ratio (reciprocal of specific impedance ratio) as low as $\beta = .002$ can be measured with some confidence, provided that corrections are applied for wind and temperature gradients. These corrections have been derived as part of the present study (Chapter 7).

The principal drawback to the broad-band measurement is the difficulty of extracting information on frequency dependence. Further work is required to demonstrate the feasibility of extracting such information from the broad-band recordings. This avenue seems promising, and the required analysis ought to be undertaken.

10.2 Results of Impedance Measurement

Table 7 presents a comparison of the specific admittance ratios as measured by the various techniques, for a particular frequency (1000 Hz). (Clearly the broad-band result is available only as a value averaged over the frequency band 100-2500 Hz.) The observed discrepancies are readily explained by the limitations of each technique, as discussed above. Thus, for the unsealed asphalt, the phase measurement with the impedance tube is not reliable because of the sensitivity to small imprecision in the measurement of the position of the minimum. Conversely, the measurement of $|\beta|$ using the pure tone traverse may well be limited by the ability to measure low values of $|\beta|$ with this technique. The accelerometer, of course, measures only the mechanical portion of the admittance, and sets a lower bound to $|\beta|$. The phase also refers only to the mechanical portion of the specific admittance.

The most reliable values of the specific admittance ratio of the unsealed asphalt are felt to be those obtained from the impedance tube data, $|\beta| = .03 \pm .01$. (Data using the broad-band technique were not taken for the unsealed asphalt due to unexpectedly high ambient noise conditions.) The more reliable phase measurements are believed to be those obtained from the traverse, ranging from -5° to -70° . No confidence interval has been established for this measurement, although known imprecision in position measurement limits the accuracy of these results to $\pm 5^\circ$.

For the sealed asphalt, the broadband results are believed to be the most reliable. These average to $\beta = .007 \pm .004$. The value .004 is the standard deviation of the 30 measurements about the mean. Systematic effects of source directivity and temperature gradients (which might shift the mean value of β) have not been included. These uncertainties in systematic effects can be reduced in future measurements by greater control of the source, and by careful measurement of temperature gradients. The phase of C_r , deduced from comparison of measured cross-correlograms with theoretically predicted correlograms, is believed to be $0^\circ \pm 10^\circ$, averaged over frequency. Traverse data for the sealed asphalt was not available for comparison due to adverse weather at the time of the scheduled test.

Table 7. MEASURED SPECIFIC ADMITTANCE RATIO AT 1000 HZ

	UNSEALED ASPHALT		SEALED ASPHALT	
	$ \beta $	$\arg \beta$	$ \beta $	$\arg \beta$
IMPEDANCE TUBE	.03	+25°	.02	+79°
ACCELEROMETER	--	--	.0003	-30°
PURE-TONE TRAVERSE	.06	-70°	--	--
PULSE-ECHO	.00	XX	.01	XX
BROAD-BAND* CROSS-CORRELATION	--	XX	.007	XX

*(BROAD BAND VALUES OF β)

NOTE: XX indicates quantities which cannot be obtained using the methods of this study.
 -- indicates that data were not obtained during this study.

10.3. Effect of Impedance on Source Emission Measurements

Analysis of the effects of surface impedance on noise source emission measurements (Section 9) suggests that uncertainties of 1-2 dB including systematic errors as high as 1 dB can be expected in typical measurements conducted on a surface with a specific admittance ratio β of .01. The broadband measurement technique is certainly capable of measuring values of β as low as .01; and, by controlling source directivity, reliable determinations of β (obtained by averaging a number of individual measurements) as low as .002 to .005 are to be expected. (Clearly, the "reliability" of such determinations depends also on the validity of the model.)

Correction of source emission measurements for surface impedance effects appears impractical. Frequency-dependent effects are far too sensitive to instantaneous air turbulence conditions. The systematic (frequency-independent) effects ($e_{\beta} \approx -9 \beta / \sin \alpha_i$) require knowledge of the source location to determine the angle of incidence; for complex sources such as trucks, which radiate from several areas, location of a dominant source is not well defined. Meaningful systematic corrections based on large distributed sources would be expected to be substantially less than 1 decibel. For small sources close to the ground, such as truck tires, motorcycles, or lawnmowers, the corrections would be both larger and more reliable.

For truck passby measurements, the importance in measuring the surface impedance lies in being able to bound the uncertainty in source emission measurements resulting from uncertainty in the acoustical characteristics of the test site.

Additional corrections for spherical wavefronts such as have been described in Section 8 become important only for values of the specific admittance ratio $\beta > .01$ or for angles of incidence $\alpha < 5^\circ$; both of these are considered unlikely for source emission measurements on concrete or sealed asphalt, and for which the microphone is at 1.2 m.

10.4. Further Possibilities

Further work on the broadband cross-correlation technique seems desirable. By controlling source directivity, a precision of $\pm .002$ on β (standard deviation of individual measurements of β) appears achievable. Such a careful measurement of β at the Sandusky test site may well indicate that a value of β lower than .01 is appropriate. The knowledge that β is much less than .01 would allow the estimate of uncertainties in source emission measurements due to uncertainties in site impedance to be reduced from the 1-2 dB suggested in the present study.

Extraction of frequency dependence from the broad-band data appears a practical possibility, based on a preliminary theoretical examination of the problem. The analysis required to develop this technique should be performed.

Frequency dependence of impedance, together with actual source spectra, can be combined to provide a more rigorous estimate of source emission measurement errors due to finite impedance effects. Such analysis is also desirable.

Surface impedance measurements ought to be performed at a variety of test sites and under differing pad temperature conditions to gauge the variability of the surface impedance. Measurements should also be performed at several points on the same test pad, to evaluate the variability of the surface impedance from point to point at a given site. The data base thus acquired would help to specify a pad qualification requirement. It could also show whether careful specification of pad surface construction may guarantee the required acoustical performance without the need for a rigorous qualification test.

Appendix A - Symbols

Note that the phase convention used in this paper defines the time dependence of a wave by $e^{-i\omega t}$. Some authors use a plus sign, with resulting sign inversions in ϕ_r and in $\arg \beta$. Note that A^* denotes the complex conjugate of A .

a	dimensionless inverse distance parameter [Eq.(8-2)]
a'	a/f
A_1, A_2	amplitude of first and second correlogram peaks
A_d, A_r	pressure amplitude of direct and reflected waves
$A(\omega)$	Fourier transform of p(t)
B	$(\omega_2 - \omega_1)/2\pi$ (bandwidth)
c	speed of sound in air
c_0	speed of sound in air at ground level
c'	$c_0 + w \cos \theta$ (speed of sound in wind)
C_1	constant of integration [Eq.(7-21)]
C_r	reflection coefficient of test surface (at some angle of incidence), for spherical wavefront [defined by Eq.(1-1)]
$ C_r $	magnitude of C_r
C_{rp}	reflection coefficient of test surface, for plane waves
ds	element of path length
D_1	distance from test surface to first minimum (impedance tube)
e_β	error in measured source emission level as a result of test pad surface having a specific admittance ratio of β rather than 0
f	frequency
f_0	$(\omega_2 + \omega_1)/4\pi$ (center frequency)
F(a)	Ingard's integral [Eq.(8-2c)]
h	microphone height

H	source height
i	$\sqrt{-1}$
$I_w(z)$	wind integral [Eq.(7-13)]
k	$2\pi/\lambda$ (wave number)
K_1, K_2, K_3	coefficients used in wind corrections, Eqs. (7-45, 46, 47)
M_w	wind correction factor for focusing effect: ratio of pressure amplitude in the presence of wind to the amplitude in still air [Eq.(7-31)]
n	positive integer
p	(acoustic) pressure
$p_1(t), p_2(t)$	pressure time histories of two sound signals
p^w	acoustic pressure in the presence of wind
p^o	acoustic pressure in the absence of wind
r	horizontal distance between source and microphone
r'	"adjusted" r [Eq.(3-1)]
$r_{ss}(\tau)$	normalized "source" (near-field) autocorrelation function, $R_{ss}(\tau)/R_{ss}(0)$
R_1	slant distance from source to microphone: $R_1 = [r^2 + (H-h)^2]^{1/2}$
R_2	slant distance via reflected ray, from source to microphone: $R_2 = [r^2 + (H+h)^2]^{1/2}$
R_s	distance from source to near-field microphone
R_1^c, R_2^c	R_1, R_2 as measured in coordinate system comoving with the wind (Section 7.2).
$R_{12}(\tau)$	cross-correlation function between $p_1(t)$ and $p_2(t)$.
$R_{ss}(\tau)$	"source" (near-field) autocorrelation function
sign(ω)	sign function: = 1 if ω is positive, -1 if negative, 0 if zero.

t	time (as a parameter)
T	Propagation time (esp. Section 7); also used as length of available time history [Eq. (5-1); Appendix C]
T_{pulse}	Pulse width [Eq.(4-2)]
T_1, T_2	propagation time of direct and reflected rays, respectively
T^w	propagation time in the presence of wind (also $T_{\text{dir}}^w, T_{\text{refl}}^w$)
T^0	propagation time in the absence of wind (also $T_{\text{dir}}^0, T_{\text{refl}}^0$)
w	wind speed; also specifically wind speed in the direction of propagation
$w(z)$	same, expressed explicitly as a function of height z
w^T	equivalent wind profile, i.e., that wind profile which causes the same effects as a given temperature profile [Eq.(7-6)]
w-function	in Eq.(8-3), as defined in Ref. 35 - related to error function
x	horizontal coordinate in plane of propagation
x_1	horizontal distance from source to reflection point
x_2	horizontal distance from reflection point to microphone: $x_2 = r - x_1$
z	specific acoustic impedance
z	vertical coordinate (distance above surface)
$z(x)$	propagation path, expressed as height as a function of distance
z'	dz/dx
z_0	$z(0)$
z_0'	$z'(0)$
z_p	value of $z(x)$ at highest (or lowest) point on direct ray path
z_e'	dz/dx at source

α	angle of incidence, measured from the horizontal. In general, angle of the ray path with the horizontal
$\alpha(z)$	same, with explicit dependence on height z (in the presence of gradients)
α_i	angle of incidence, measured from the horizontal $\alpha_i = \alpha(0)$
α_i^w	α_i in the presence of wind
α_i^o	α_i in the absence of wind
α_r	$\alpha(z)$ at the microphone
α_r^w, α_r^o	α_r in the presence, absence of wind, respectively
β	specific acoustic admittance ratio $\rho c/z$
β^w	β inferred from C_r and including wind effects in the computation
β^o	same, not including wind effects
β^p	β inferred from C_r using the plane-wave approximation $C_r = C_{rp}$ [Eq. (8-4)]
γ	$\sin \alpha$
γ_d, γ_r	γ for direct and reflected waves, respectively
δ	propagation time difference between direct and reflected rays, in cross-correlation configuration; same as $\delta\tau$
δ_{comp}	value of δ computed from source/microphone geometry, with or without wind effects.
δ_{meas}	value of δ obtained from cross-correlogram
δ_R	path length difference between direct and reflected ray: $\delta_R = R_2 - R_1$
δT	(used in Fermat's principle, Section 7) - change in propagation time T resulting from an infinitesimal change in the propagation path, keeping the end points fixed
δx_1	infinitesimal change in x_1 as a result of following a "neighboring" ray rather than the original ray. Similarly $\delta z_e', \delta z_r, \delta z_r^w, \delta z_r^o, \delta z_o', \delta \alpha_i$

$\delta\tau$	propagation time difference between direct and reflected rays: $\delta\tau = (R_2 - R_1)/c$ in the absence of wind
$\delta\tau^w, \delta\tau^o$	$\delta\tau$ in the presence or absence of wind, respectively
Δ	difference in propagation time between direct rays to near-field and far-field microphones, in cross-correlation configuration; $\Delta = (R_1 - R_s)/c$ in the absence of wind
ΔL	difference in levels between maximum and minimum (impedance tube or traverse)
$\theta(z)$	temperature profile (function of height z)
θ	angle between wind direction and horizontal component of direction of propagation of the sound signal
λ	wavelength
λ	parameter used in proof of time-of-flight lemma [Eq.(7-7)] λ is set equal to w/c to complete the proof
$\tilde{\lambda}, \bar{\lambda}$	specific values of the parameter λ , arising from application of Taylor's theorem
ρ	density of air
ρc	specific acoustic impedance of air
σ	standard deviation of a set of measurements; for n measurements x_i , $\sigma = \sqrt{\frac{\sum (x_i - \bar{x})^2}{n-1}}$ where $\bar{x} = \sum x_i/n$ is the mean
ϕ_r	$\arg C_r$: phase of reflection coefficient
ϕ	phase difference between direct and reflected ray, at microphone
ϕ_o	that part of ϕ attributable to geometry: $\phi_o = 2\pi(R_2 - R_1)/\lambda$
ψ	velocity potential [Eq.(8-2a)]; $p = \partial\psi/\partial t$
ω	angular frequency: $\omega = 2\pi f$
ω_1, ω_2	lower and upper limits of ω for band-limited signal

Appendix B

Results have been expressed in terms of the specific acoustic admittance ratio β ($\beta = \rho c/z$) rather than its inverse ζ (used in earlier reports*), for several reasons. First, the plane-wave reflection coefficient can be written as $C_r = 1 - 2\beta/\alpha +$ small corrections of order $(\beta/\alpha)^2$, for the small values of specific admittance ratio β and the glancing angles α of interest. Thus, errors in the measured quantity C_r propagate linearly in computing β , and therefore it appears more reasonable to average the values of β obtained from repeated measurement of C_r rather than averaging ζ . Similarly, data scatter as measured by the standard deviation of β 's is considered to be more meaningful, again because of the linear relationship with the measured quantity C_r . Also, since values of $|C_r|$ greater than 1 arise from inaccuracies in measurement, these determinations of C_r must not be discarded when computing the mean and measures of scatter of the data. By computing β , rather than ζ , one avoids introducing a discontinuity at $C_r = 1$ ($\beta = 0$), thereby allowing inclusion of the measurements for which $|C_r| > 1$ in the determination of the mean and standard deviation of β . Finally, theoretical analyses such as "finite impedance" (spherical wavefront) corrections seem more naturally expressed in terms of the small number β .

*Letter reports to the U.S. Environmental Protection Agency dated November 1, 1976, and December 14, 1976.

The following conventions regarding Fourier representations will be observed. To avoid confusion, the convention of discarding the imaginary part of complex quantities will not be presumed; it must be stated explicitly.

Thus, $Ae^{-i\omega t}$ does not represent the sound pressure of a pure tone: sound pressure must be real, whereas $e^{-i\omega t}$ is complex. $A(e^{-i\omega t} + e^{i\omega t}) = 2A \cos \omega t$ is real and represents a pure tone.

For arbitrary sound pressure $p(t)$,

$$p(t) = \int_{-\infty}^{\infty} A(\omega) e^{-i\omega t} d\omega \quad (\text{C-1})$$

and hence

$$A(\omega) = \frac{1}{2\pi} \int_{-\infty}^{\infty} p(t) e^{+i\omega t} dt \quad (\text{C-2})$$

Since $p(t)$ is real, $A(-\omega) = A^*(\omega)$, where the asterisk denotes complex conjugate. By changing ω to $-\omega$ in Eq. (C-1) and applying $A(-\omega) = A^*(\omega)$,

$$p(t) = \int_{-\infty}^{\infty} A^*(\omega) e^{+i\omega t} d\omega \quad (\text{C-3})$$

as well. The identity

$$\int_{-\infty}^{\infty} e^{-i\omega t} dt = 2\pi\delta(\omega) \quad (\text{C-4})$$

is required. With two pressure signals p_1 and p_2 , their Fourier transforms will be distinguished by A_1 and A_2 , respectively.

The cross-correlation function $R_{12}(\tau)$ is then

$$R_{12}(\tau) = \frac{1}{T} \int_{-T/2}^{T/2} dt p_1(t) p_2(t+\tau) \quad (\text{C-5})$$

where the limit $T \rightarrow \infty$ will be taken freely. Writing

$$p_1(t) = \int_{-\infty}^{\infty} A_1^*(\omega) e^{+i\omega t} d\omega \quad (\text{C-6a})$$

$$p_2(t+\tau) = \int_{-\infty}^{\infty} A_2(\omega) e^{-i\omega' t} e^{-i\omega' \tau} d\omega' \quad (\text{C-6b})$$

and substituting gives

$$R_{12}(\tau) = \frac{1}{T} \int_{-\infty}^{\infty} dt \int_{-\infty}^{\infty} d\omega \int_{-\infty}^{\infty} d\omega' A_1^*(\omega) A_2(\omega') e^{-i(\omega' - \omega)t} e^{-i\omega'\tau}. \quad (C-7)$$

Interchanging the order of integration and performing the integration over t gives

$$R_{12}(\tau) = \frac{2\pi}{T} \int_{-\infty}^{\infty} d\omega \int_{-\infty}^{\infty} d\omega' A_1^*(\omega) A_2(\omega') \delta(\omega' - \omega) e^{-i\omega'\tau}, \quad (C-8)$$

using Eq.(C-4). The ω' integration gives

$$R_{12}(\tau) = \frac{2\pi}{T} \int_{-\infty}^{\infty} d\omega A_1^*(\omega) A_2(\omega) e^{-i\omega\tau}. \quad (C-9)$$

For the case of band-limited white noise from a point source,

$$A(\omega) = \begin{cases} \frac{A}{4\pi R} e^{+i\omega R/c} & (\omega_1 \leq |\omega| \leq \omega_2) \\ 0 & (\text{otherwise}) \end{cases}, \quad (C-10)$$

where ω_1 and ω_2 are the lower and upper frequency limits of the noise, R is the distance from the source, and A is a measure of source energy per unit ω (A is real). As usual, frequency (Hz) is given by $f = \omega/2\pi$. At the near-field microphone, $R = R_s$. At the far-field microphone, the reflected wave must be included:

$$\begin{aligned} A_2(\omega) &= \frac{A}{4\pi R_1} e^{i\omega R_1/c} + C_r(\omega) \frac{A}{4\pi R_2} e^{i\omega R_2/c} \\ &= \frac{A}{4\pi R_1} e^{i\omega R_1/c} + |C_r(\omega)| \frac{A}{4\pi R_2} e^{i\omega R_2/c + i\phi_r(\omega)}, \end{aligned} \quad (C-11)$$

where R_1 and R_2 are the distance from the source and its image, respectively. The assumption that C_r is independent of frequency is now applied. However, the requirement that $\bar{A}(-\omega) = A^*(\omega)$ -- necessary because $p(t)$ must be real -- forces $C_r(-\omega) = C_r^*(\omega)$, i.e., $\phi_r(-\omega) = -\phi_r(\omega)$. Thus, even for C_r independent of frequency, $\phi_r(\omega) = \text{sign}(\omega) \frac{\pi}{2} \text{const.}$ (From a physical standpoint one would consider only positive frequencies, $\omega > 0$. The spectral decomposition looks like $A(\omega) + A(-\omega)$, and the reflected signal looks like $|C_r| \cos(\omega R_2/c + \phi_r - \omega t)$, where now ϕ_r is independent of frequency.)

Substituting Eqs. (C-10) and (C-11) into (C-9) gives

$$\begin{aligned}
 R_{12}(\tau) &= \frac{2\pi}{T} \int_{\omega_1}^{\omega_2} d\omega \frac{A^2}{4\pi^2 R_s} e^{-i\omega R_s/c} \left(\frac{1}{R_1} e^{i\omega R_1/c} + \right. \\
 &\quad \left. \frac{|C_r|}{R_2} e^{i\omega R_2/c + i\phi_r} \right) e^{-i\omega\tau} \\
 &+ \frac{2\pi}{T} \int_{-\omega_2}^{-\omega_1} d\omega \frac{A^2}{4\pi^2 R_s} e^{-i\omega R_s/c} \left(\frac{1}{R_1} e^{i\omega R_1/c} + \right. \\
 &\quad \left. \frac{|C_r|}{R_2} e^{i\omega R_2/c - i\phi_r} \right) e^{-i\omega\tau} \quad (C-12) \\
 &= \frac{2A^2}{4\pi R_s T} \left\{ \frac{1}{R_1} \frac{\sin \pi B(\Delta - \tau)}{\Delta - \tau} \cos 2\pi f_o(\Delta - \tau) + \right. \\
 &\quad \left. \frac{|C_r|}{R_2} \frac{\sin \pi B(\Delta + \delta - \tau)}{\Delta + \delta - \tau} \cos \left[2\pi f_o(\Delta + \delta - \tau) + \phi_r \right] \right\},
 \end{aligned}$$

where now B is the bandwidth $(\omega_2 - \omega_1)/2\pi$; f_o is the center frequency $(\omega_2 + \omega_1)/4\pi$; Δ is the propagation time difference between the near-field and far-field microphone, of the direct signal: $\Delta = (R_1 - R_s)/c$; and δ is the time difference, $(R_2 - R_1)/c$, between direct and reflected signals to the far microphone.

In computing the source autocorrelation, both p_1 and p_2 are given by Eq. (C-10). Then

$$R_{ss}(\tau) = \frac{2A^2}{4\pi R_s T} \frac{\sin \pi B\tau}{\tau} \cos 2\pi f_o\tau. \quad (C-13)$$

Thus, for the case $\phi_r = 0$, Eq.(C-12) can be rewritten as

$$R_{12}(\tau) = \frac{R_s}{R_1} \left\{ R_{ss}(\Delta - \tau) + |C_r| \frac{R_1}{R_2} R_{ss}(\Delta + \delta - \tau) \right\}. \quad (C-14)$$

The ratio of correlogram peaks is thus

$$\frac{A_2}{A_1} = \frac{R_{12}(\Delta + \delta)}{R_{12}(\Delta)} = \frac{r_{ss}(\delta) + |C_r| R_1/R_2}{1 + r_{ss}(\delta) |C_r| R_1/R_2} \quad (C-15)$$

where $r_{ss}(\tau) = R_{ss}(\tau)/R_{ss}(0)$ is the normalized source autocorrelation function, and the identity $R_{ss}(-\tau) = R_{ss}(\tau)$, which follows directly from Eq. (C-5) if $p_1 = p_2$, has been used.

In generating correlograms, both by using the cross-correlation analyzer and by modeling on a high-speed computer, the normalized cross-correlation function has been used. The normalization is performed with respect to the root-mean-squared signal amplitudes:

$$r_{12}(\tau) = \frac{R_{12}(\tau)}{\sqrt{R_{11}(0) R_{22}(0)}} \quad , \quad (C-16)$$

where $p_1(\text{rms}) = \sqrt{R_{11}(0)}$ follows from Eq. (C-5). Thus the actual sound pressure level is factored out of the normalized correlograms. In the presence of noise, the rms amplitudes increase, but $R_{12}(\tau)$, for τ near Δ , is unchanged. Thus the amplitude of $r_{12}(\tau)$ decreases, but its shape (and relative peak heights) remains the same.

Appendix D. Exact Ray Path Integral

From Eq. (7-23), the ray path in the presence of wind is described by

$$x = \int_0^z \frac{dz}{\sqrt{z_0'^2 - 2w(z)/c_0}} \quad (D-1)$$

For the case $w(z) \propto z^{1/n}$, this can be integrated analytically to give

$$x = 2n \frac{z}{z_0}, \left(\frac{c_0 z_0'^2}{2w(z)} \right)^n \sum_{r=0}^{n-1} \frac{(-1)^r (n-1)!}{(2r+1)r!(n-1-r)!} \left[1 - \left(1 - \frac{2w(z)}{c_0 z_0'^2} \right)^{r+\frac{1}{2}} \right] \quad (D-2)$$

(setting $y = z^{1/n}$ and using Integral 134 in Ref. 36).

Numbered List of References

1. Environmental Protection Agency Noise Emission Standards for New Medium and Heavy Duty Trucks, U.S. Federal Register, 41, Section 205.54, p. 15544 (April 13, 1976).
2. Holmer, C.I., and Kilmer, R.D., A Proposed Experiment to Evaluate Environmental Dependence of the Measurement of Noise from Medium and Heavy Duty Trucks, NBS Report NBSIR 76-1138 (National Bureau of Standards, September 1976).
3. Morse, P.M., and Ingard, U., *Theoretical Acoustics*, pp. 259-270 (McGraw-Hill, Inc., New York, 1968).
4. Shaw, E.A.G., The Acoustic Waveguide. II. Some Specific Normal Acoustic Impedance Measurements of Typical Porous Surfaces with Respect to Normally and Obliquely Incident Waves, *J. Acoust. Soc. Am.* 25 (2), 231-235 (March 1953).
5. Attenborough, K., The Prediction of Oblique-Incidence Behaviour of Fibrous Absorbents, *J. Sound Vib.* 14 (2), 183-191 (1971).
6. Beranek, L.L., *Acoustic Measurements*, pp. 309-325 (John Wiley & Sons, Inc., New York, 1949).
7. Standard Method of Test for Impedance and Absorption of Acoustical Materials by the Tube Method, ASTM C384-58 (R1972), in 1977 Annual Book of ASTM Standards, Part 18 (American Society for Testing and Materials, Philadelphia, 1977).
8. Chang, Y.M., The Acoustic Absorption Coefficients and Impedances of the Test Pads of the U.S. Environmental Protection Agency Noise Enforcement Facility, Sandusky, Ohio (Draft), EPA report 336/9-77-001 (U.S. Environmental Protection Agency Noise Enforcement Facility, Sandusky, Ohio, October 1976).
9. Embleton, T.F.W., Piercy, J.E., and Olson, N., Outdoor Sound Propagation Over Ground of Finite Impedance, *J. Acoust. Soc. Am.* 59 (2), 267-277 (Feb. 1976).
10. Jaeger, E.W., Oblique-Angle Determination of the Reflection Coefficient R of Flat Sound Absorbers, *J. Acoust. Soc. Am.* 54 (1), 280(A) (July 1973).
11. Daigle, G.A., Piercy, J.E., and Embleton, T.F.W., Degraded Interference between Directional Ground-Reflected Sound Waves Due to Atmospheric Turbulence, *J. Acoust. Soc. Am.* 61, Suppl. 1, p. S14(A) (Spring, 1977).

12. Gatley, W.S., and Cohen, R., Methods for Evaluating the Performance of Small Acoustic Filters, *J. Acous. Soc. Am.* 46, 6-16 (1969).
13. Spandöck, F., Experimentelle Untersuchung der akustischen Eigenschaften von Baustoffen durch die Kurztonmethode. *Ann. Physik*, 5, 328-338 (1934).
14. Walker, B., and Delasso, L.P., Integrated Pulse Technique for the Measurement of Acoustical Absorption Techniques. Seventh International Congress on Acoustics, Budapest, 1971.
15. Rogers, C.L., and Watson, R.B., Determination of Sound Absorption Coefficients Using a Pulse Technique, *J. Acous. Soc. Am.* 32 (12), 1555-1558 (Dec. 1960).
16. Powell, J.G., and Van Houten, J.J., A Tone-Burst Technique of Sound-Absorption Measurement. *J. Acous. Soc. Am.* 48, 1299 (1970).
17. Tsau, M.C.C., and Musa, R.S., Transient and Steady State Sound Absorption Coefficients of Fiberglass and Polyurethane Foam. *Inter-Noise 72 Proceedings* pp. 445-450. (Wash., D.C., Oct. 1972).
18. Lapin, L.L., *Statistics for Modern Business Decisions*, p. 353-365 (Harcourt Brace Jovanovich, Inc., New York 1973).
19. Bendat, J.S., and Piersol, A.G., *Random Data: Analysis and Measurement Procedures* (John Wiley & Sons, New York, 1971)
20. Seybert, A.F., and Ross, D.F., Experimental Determination of Acoustic Properties Using a Two-Microphone Random-Excitation Technique. *J. Acous. Soc. Am.* 61 (5), 1362-1370 (May 1977).
21. Hollin, K.A., and Jones, M.H., The Method of Sound Absorption Coefficient in Situ by a Correlation Technique. *Acustica* 37(2), 103-110 (March 1977).
22. Fowweather, F., Hollin, K.A., and Jones, M.H., The Measurement of Absorption Coefficient Using a Correlation Technique. Presented at British Acoustical Society Meeting, Sept. 1971.
23. Schomer, P.D., Measurement of Sound Transmission Loss by Combining Correlation and Fourier Techniques. *J. Acous. Soc. Am.* 51 (4), 1127-1141 (Apr. 1972).
24. Goldstein, H., *Classical Mechanics*, pp. 231, 312 (Addison-Wesley Publishing Co., Reading, Mass., 1959).

U.S. DEPT. OF COMM. BIBLIOGRAPHIC DATA SHEET	1. PUBLICATION OR REPORT NO. NBSIR 78-1541	2. Gov't Accession No.	3. Recipient's Accession No.
4. TITLE AND SUBTITLE Techniques for the Measurement of Acoustic Impedance of Asphalt		5. Publication Date October 1978	
7. AUTHOR(S) Peter A. Mansbach, Curtis I. Holmer		6. Performing Organization Code	
9. PERFORMING ORGANIZATION NAME AND ADDRESS NATIONAL BUREAU OF STANDARDS DEPARTMENT OF COMMERCE WASHINGTON, D.C. 20234		8. Performing Organ. Report No.	
12. Sponsoring Organization Name and Complete Address (Street, City, State, ZIP) Environmental Protection Agency Office of Noise Abatement and Control Crystal Mall #2 Washington, D. C. 20460		10. Project/Task/Work Unit No. 2004457	
15. SUPPLEMENTARY NOTES		11. Contract/Grant No. EPA-1AG-D6-0755	
16. ABSTRACT (A 200-word or less factual summary of most significant information. If document includes a significant bibliography or literature survey, mention it here.) Five techniques were used in an attempt to measure the very high acoustic impedance of an asphalt surface. These techniques are: Impedance Tube, Pure-Tone Traverse, Pulse-Echo, Broad-Band Cross-Correlation, and Direct Accelerometer Measurement. These techniques are described and evaluated in some detail, and the results of the measurements are presented. Of the five techniques, the broad-band cross-correlation proved to be the most effective, and also is capable of even further improvement. The value of the specific acoustic admittance of the sealed asphalt surface obtained with this technique is .007. The effects of wind and temperature gradients on ray propagation are derived theoretically, as well as spherical wavefront corrections to plane-wave reflection. These refinements are necessary to realize the full potential of the broad-band measurement technique. Effects of the finite test surface impedance on source emission measurements are discussed. Measurement uncertainties of the order of 1-2 dB due to surface impedance are considered likely.		13. Type of Report & Period Covered Final Aug. 76-Mar. 77	
17. KEY WORDS (Six to twelve entries; alphabetical order; capitalize only the first letter of the first key word unless a proper name, separated by semicolons) Acoustics; acoustic impedance of asphalt; correlation, used to measure acoustic impedance; Fermat's principle in acoustics; impedance, acoustic, measurement of; impedance, acoustic, of asphalt; noise measurement, truck passby; sound propagation, in wind gradients; sound propagation over impedance surface; wind gradients, effect on sound propagation.		14. Sponsoring Agency Code	
18. AVAILABILITY <input checked="" type="checkbox"/> Unlimited <input type="checkbox"/> For Official Distribution. Do Not Release to NTIS <input type="checkbox"/> Order From Sup. of Doc., U.S. Government Printing Office Washington, D.C. 20402, SD Cat. No. C13 <input type="checkbox"/> Order From National Technical Information Service (NTIS) Springfield, Virginia 22151	19. SECURITY CLASS (THIS REPORT) UNCLASSIFIED	21. NO. OF PAGES 104	
		20. SECURITY CLASS (THIS PAGE) UNCLASSIFIED	22. Price \$6.50

